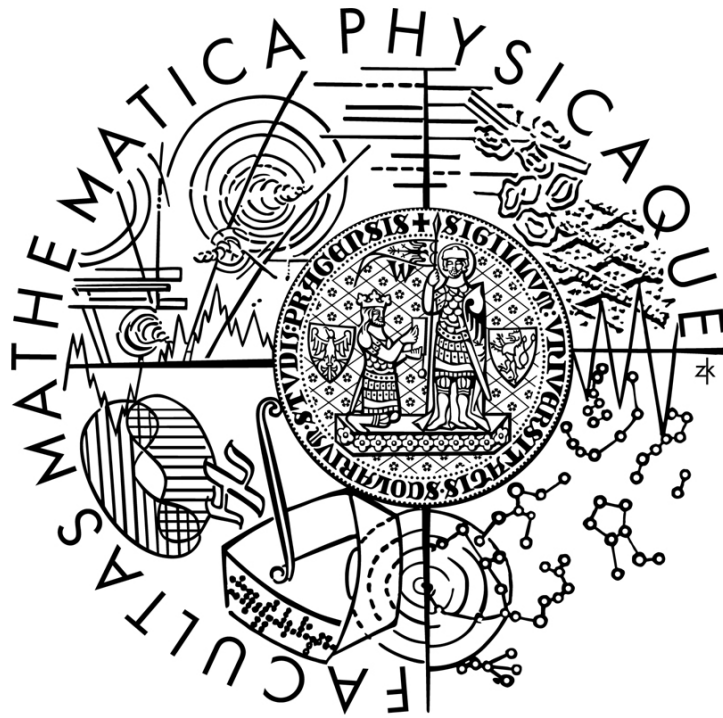


Univerzita Karlova v Praze
Matematicko-fyzikální fakulta

DIPLOMOVÁ PRÁCE



Peter Darebník

Studium a využití povrchových plazmonů v terahertzové spektrální oblasti

Katedra chemické fyziky a optiky

Vedoucí diplomové práce: doc. RNDr. Petr Kužel, Dr.

Studijní program: Fyzika

Studijní obor: Optika a optoelektronika

Praha 2016

Prohlašuji, že jsem tuto diplomovou práci vypracoval samostatně a výhradně s použitím citovaných pramenů, literatury a dalších odborných zdrojů.

Beru na vědomí, že se na moji práci vztahují práva a povinnosti vyplývající ze zákona č. 121/2000 Sb., autorského zákona v platném znění, zejména skutečnost, že Univerzita Karlova v Praze má právo na uzavření licenční smlouvy o užití této práce jako školního díla podle § 60 odst. 1 autorského zákona.

V Praze dne

Peter Darebník

Název práce: Studium a využití povrchových plazmonů v terahertzové spektrální oblasti

Autor: Peter Darebník

Katedra: Katedra chemické fyziky a optiky

Vedoucí diplomové práce: doc. RNDr. Petr Kužel, Dr., Katedra chemické fyziky a optiky – externí pracovník

Abstrakt: Cílem této práce je analytické, numerické, a experimentální studium povrchových plazmonů v terahertzové spektrální oblasti.

Popis šíření plazmonu na rozhraní kov/dielektrikum je možné provést zcela analyticky. Naším cílem je získat popis povrchového plazmonu který vzniká ve složitějších anizotropních dielektrických vrstevnatých strukturách v kontaktu s kovovou vrstvou. Analýzu disperzních rovnic plasmonu v anizotropní vrstevnaté struktuře jsme provedli pomocí numerických výpočtů. Existující experiment transmisní terahertzové spektroskopie jsme rozšířili o uspořádání, které umožňuje navázat povrchový plasmon na kovovou podložku a měřit jeho charakteristiky při průchody vzorky v kontaktu s touto podložkou. Získaná teoretická i experimentální data byla následně vyhodnocena abychom mohli určit do jaké míry lze šíření povrchového plazmonu využít pro spektroskopii v terahertzovém oboru.

Závěrem konstatujeme, že se nám podařilo popsat povrchové plasmony ve vrstevnatých prostředích včetně anizotropních vrstev a dospěli jsme k závěru že povrchové plasmony by mohly být uplatnitelné v spektroskopii v terahertzové spektrální oblasti pro měření odezvy dielektrických materiálů ve směru kolmém k jejich povrchu.

Klíčová slova: Plazmon, Plazmová frekvence, Drudeho permitivita kovů, Formalizmus přenosových matic

Title: Study and application of surface plasmons in terahertz spectral range

Author: Peter Darebník

Department: Department of Chemical Physics and Optics

Supervisor: doc. RNDr. Petr Kužel, Dr., department of Chemical Physics and Optics – external employee

Abstract: The goal of this thesis is analytical, numerical and experimental study of surface plasmons in terahertz spectral range

The description of the surface plasmon propagation along metal/dielectric interface can be done purely analytically. Our goal is to obtain the description of the surface plasmon propagating in more complex dielectric layered structures which are in contact with metallic layer. Analysis of the surface plasmon dispersion curves in anisotropic layered structure was done numerically. Existing transmission terahertz spectroscopy experiment was expanded by an arrangement that allows us to excite the surface plasmon on the metallic layer and allows us to measure its characteristics after the transmission of samples, that are in contact with this layer. Obtained theoretical and experimental data were then evaluated, so we could conclude to which extent can the surface plasmon be used for spectroscopic purposes in terahertz range.

We concluded, that we were able to describe surface plasmons in layered structures including anisotropic layers and that we believe the surface plasmons could be applicable in the spectroscopy in the terahertz spectral range for the purposes of the measurement of the out-of-plane response of dielectric materials.

Keywords: Plasmon, Plasmonic frequency, Drude permittivity of metals, Transfer matrix formalism

Rád by som sa poďakoval doc. RNDr. Petrovi Kuželovi, Dr. za rozsiahlu pomoc pri písaní tejto diplomovej práce, bez ktorej by ju nebolo možné dokončiť. Taktiež by som sa chcel poďakovať celému oddeleniu dielektrík Fyzikálneho Ústavu AV ČR, v. v. i. za sprístupnenie laboratória pre potreby merania experimentálnej časti tejto práce. Ďakujem tiež pani Helene Kisvetrovej sa pomoc s oficiálnymi náležitosťami tejto práce. V neposlednom rade patrí vďaka celej mojej rodine za neprestajnú podporu a pomoc.

Table of Contents

Preface	7
Introduction into surface plasmon polaritons	9
1. Surface plasmons in optics	9
2. Surface plasmon coupling methods in THz spectral range	10
Motivation	14
1. Theoretical background	16
1.1 Drude model and permittivity	16
1.2 Transfer matrix formalism and its relation to guided modes	18
1.3 Conclusion	22
2. Surface plasmon polariton calculation via TMF	23
2.1 Metal/isotropic dielectric interface	23
2.2 Metal/anisotropic dielectric interface	26
2.2.1 TMF for the anisotropic medium	26
2.2.2. Solution of the condition (29)	28
2.3 SPP in an isotropic dielectric layer deposited on a metallic surface	30
2.4 SPP in an anisotropic dielectric layer deposited on a metallic surface	31
2.5 Solution of condition (41) and (44).	32
2.6. Conclusion	34
3. Graphical representation of theoretical research	35
3.1 Metal/isotropic dielectric interface	35
3.2. Metal/anisotropic dielectric interface	38
3.3. SPP in a dielectric layer	41
3.3.1. isotropic layer	42
3.3.2. anisotropic layer	46
3.4. Conclusion	48
4. Numerical solution of SPP propagation	49

4.1. The basics	51
4.2. Generating the wave	52
4.3. Results	56
4.6. Conclusion	64
5. The experiment	66
5.1. Metal/isotropic dielectric interface results	69
5.2 Measurements on Si, ZnTe, GaAs and LGO samples	71
5.3. Conclusion	75
Thesis conclusion	76
References	78

Preface

It is known that light can either propagate through, or reflect off of an interface between two materials, whatever they may be. Let us take for example an ordinary mirror. It is an interface between a metallic layer deposited on a glass, usually flat, surface. Visible light does obviously reflect from it, however gamma rays, for example, just pass through it.

The reason behind this are the so called plasmons. In the classical picture they can be viewed as oscillations of the electron density with respect to the fixed position of ions in the metal. These oscillations are caused by the electric field supplied by an incident wave (which changes harmonically in time), and, since the material has to be electrically neutral, the electrons rearrange because of the Lorentz force and the Coulombic interaction, to keep the net electric field in the metal zero. This can only happen up to the plasma frequency, however, since above it the electrons can not respond fast enough (because of their inertia) to screen the electric field of the wave. This translates into a small absorption of the light so it just passes through the metal. On the other hand, below the plasma frequency, the electrons' screening effect causes the wave to reflect. The plasma frequency is usually in the UV range in metals and it is denoted as ω_p .

Light can sometimes propagate along the metal/dielectric interface. In this case we talk about the so called surface plasmon polariton mode of propagation, or in short SPP, or simply surface plasmon.

While, as the name suggests, this mode of propagation is again connected to the free electrons in the material, the goal of this thesis is not to explain the elementary physics behind the phenomenon but rather to develop a new spectroscopic method. Since the SPP electric field has an out-of-plane component, an opportunity arises here to use SPP for measurements

of an out-of-plane response of dielectric materials.

The out of plane response is otherwise difficult to access by standard transmission or reflection spectroscopy because of the transverse nature of the electromagnetic radiation.

Introduction into surface plasmon polaritons

In this chapter we will have a look on a summary of work done in the field optics using the surface plasmon polariton.

1. Surface plasmons in optics

The surface plasmon excitation is known for a very long time. At the beginning of 20th century it was observed that a polarized light sent onto a metallic diffraction grating creates dark and light bands in the reflected beam [1]. A more detailed theoretical description of this phenomenon was provided by lord Rayleigh in his dynamical theory of grating [2] where he remarked that the observed anomalies are observed for the wavelengths for which one of the diffraction orders emerged from the grating at the grazing angle. Further research in 1960s has defined surface plasma oscillation localized very closely to the surface of a metal [3]. Subsequently, possibilities of optical excitation of surface plasmons using attenuated total reflections were proposed in [4] and [5].

Scientists were fascinated by the possibility, which surface plasmon offers, to confine the propagating light into sub-wavelength dimensions. Applications in the studies of the properties of thin films and chemical molecules and reaction have been developed. This gave rise to a large field of the surface plasmon sensing applications in the optical spectra region; see e.g. [6] for a review. Optical surface plasmons show a remarkable sensitivity to the refractive index of extremely thin layers and are able to detect changes due to the binding of e.g. single molecular layers. It is now possible to observe molecular interactions practically in real time [7].

The propagation of surface plasmon polaritons has been described in many publications and reviews. The propagation of surface plasmon along

a single metal/isotropic dielectric interface is now an easy exercise. The description of the propagation along the structure MIM (metal/insulator/metal) or IMI has been discussed in various publications for the isotropic case [8]. Recently MIM and IMI structures have also been studied for the case of anisotropic dielectric media [9]. In this work the dispersion relations of the surface plasmons in these structures were numerically solved for several birefringent dielectrics with the conclusion that the alignment of the birefringent material with respect to the propagation direction of the plasmon can finely tune its dispersion curve. However, the role of individual components of the permittivity tensor has not been discussed.

2. Surface plasmon coupling methods in THz spectral range

As we will show in more detail later, the surface plasmons can exist in two distinct regimes. The first is optical regime (or saturated regime as it will be called in this work) which occurs in the optical spectral range, close to the plasma frequency of metals. This regime is characterized by very high confinement of the plasmon in the perpendicular direction to the interface, and finds many sensing application as described in the previous paragraph. However these plasmons are relatively heavily damped and can propagate typically only over a few (tens) of wavelengths. The second regime appears well below the plasma frequency where the permittivity of the metal is very high and negative [10] and [11]. This so called Zenneck regime (for cylindrical symmetry – propagation along wires – one often speaks about the Sommerfeld wave) naturally occurs for example in the terahertz (THz) spectral range. In 2004 D. Mittleman [12] has remarked that THz waves can be coupled to ordinary metallic wires and transmitted over tens of

centimetres. The wave is guided by the wire despite the lossy character of the wire metal. Later on Grischkowsky has shown in [13] and [14] that in these and similar experiments one excites on the wire surface just well known Sommerfeld wave of the surface plasmon in the Zenneck regime. These discoveries have attracted interest of scientists to the „THz plasmonics,,. Zenneck plasmons behave differently than optical plasmons and may lead to different applications. Indeed, due to a small penetration depth of the electromagnetic energy into the metal, the Zenneck wave can propagate over very long distances (hundreds of wavelengths or more), however the confinement of the wave is quite small (its propagation along the surface can be disturbed by surrounding objects).

In [15] John F. O'Hara et al. proposed a mechanism of coupling and decoupling a SPP on/off a metallic surface using a grating in the surface of the metal. They have determined that while using this technique provides very rapid and efficient (>71%) coupling method its main problem is a very short lifetime and monochromaticity of the excited SPP, which limits the practical usability of launching SPPs in spectroscopic manner. They have concluded there does not seem to be an obvious solution to this problem, but there may be a system configuration that provides a favourable trade-off, where overall efficiency is reduced in favour of slower coupling and decoupling.

For possible needs of THz SPP spectroscopy a second method of SPP excitation may be used, according to mr. O'Hara and Averitt in [16].

They propose coupling the THz SPP using a silicon prism. In this method the THz pulse is incident on the prism which is placed just above the the metal's surface. The pulse then reflects inside the prism onto one of the prism's edges, causing edge diffraction coupling. The same method is used to

decouple the SPP. According to results in [16] it is possible to generate a broadband SPP with coupling and decoupling efficiencies of at least 3,5% stating, that those can be probably increased by the optimization of the experimental arrangement. They have also shown the sensitivity of the surface plasmon to dielectric tape placed onto the metallic substrate resulting into different transmittance spectrum as compared to the reference.

Consequently it would seem, that the latter method is ideal for SPP generation for the purposes of THz spectroscopy since it provides a broadband SPP and relatively high coupling and decoupling efficiencies.

With the advent of metamaterials, it became obvious that the plasma frequency of the metal can be effectively lowered by „diluting,, the metal in form of thin wires [32]. This leads to the idea of „decorating,, metal surfaces with some corrugation of sub-wavelength size in order to shift the effective plasma frequency down to far-infrared range and to tune the surface plasmon propagation and confinement also in the THz regime. In [18] J. B. Pendry et al. studied the propagation of SPP along a metallic substrate perforated by holes. They state, that the electromagnetic wave propagation is governed by an effective permittivity of such a material. Since the hole's size and spacing can be readily controlled on all relevant scales, it allows the creation of designer surface plasmons with almost arbitrary dispersion in frequency and space. In case of propagation along such a structure, we are talking about so called spoof plasmons, more closely described in [19].

In connection to [18], in [20] it is described how the dispersion relation of surface plasmon polaritons, propagating along a perfectly conducting wire, can be tailored to our needs by corrugating the surface of the wire by a periodic array of radial grooves. They conclude, that

periodically corrugated metal wires can indeed sustain spoof plasmon polaritons and that their dispersion and mode profile is determined by the geometry.

The well-known phenomenon of extraordinary transmission through sub-wavelength holes, first reported by Ebbessen in [21], is also connected to the propagation and coupling of the surface plasmon polaritons.

Lastly, in [8], long range SPPs (SPPs that can propagate over appreciable lengths – centimetres) are discussed in great detail. The extensive work talks about the application of surface plasmons in non-linear optics, bio-sensors, integrated optics and other areas.

Motivation

From the previous chapter it is obvious, that the SPPs are indeed a known phenomena. Their application and theoretical description in optics is extensively covered, however the focus of this thesis will be on THz spectral range. Even in THz range, basic theoretical description and some applications are commonly known, however it would seem, that there is no specific focus on theoretical description and spectroscopic properties of surface plasmons in this spectral range.

From [22], [23], [24] it is known that the strain is very important parameter in ferroelectric materials. It can significantly shift the temperature of the ferroelectric phase transition or induce a phase transition in a material where it would not occur under normal conditions down to 0K. This is the case for example of $SrTiO_3$, an incipient ferroelectric material, which remains in the para-electric phase down to the lowest temperature while spectroscopic measurements and first principle calculations indicate that it is in a state relatively close to the ferroelectric phase transition. Applying a tensile strain (for example by epitaxial growth of a thin film STO on a suitable substrate with slightly larger lattice constant) the ferroelectric transition appears and can be shifted close to the room temperature [22, 23]. In para-electric phase the STO single crystal is cubic. However, upon a tensile strain, the thin film material becomes tetragonal and only its in-plane dielectric component is available through standard spectroscopic techniques at high frequencies. The question is whether the surface plasmon could help with the investigations of the out-of-plane properties of the strained material.

Another example is connected to the recent theoretical developments in the field of ferroelectric domain engineering. A new oscillating mode in the THz spectral range has been predicted in a ferroelectric thin film material

with periodic 180 degrees domain structure exhibiting the spontaneous polarization perpendicular to the film surface [25]. This mode consists of oscillations of domain widths (i.e. displacement of domain walls) and, consequently, it is connected with the oscillations of the amplitude of the out-of-plane permittivity of the film, which may even become negative in a narrow interval of the terahertz frequency range [25].

Our goal in this thesis is therefore to first develop a theoretical formalism which can systematically calculate the dispersion curves for SPPs in different scenarios, such as the propagation along metal/iso(aniso)tropic dielectric film interface or propagation along metal/thin dielectric layer interface. Our next goal is to create a simple experiment in which we will try to excite a SPP and use it to do some basic spectroscopic measurements of a few selected samples.

In the course of this thesis we will therefore describe the SPPs analytically and graphically, and use this knowledge for evaluation of the experiment.

1. Theoretical background

1.1 Drude model and permittivity

In the year 1897 J.J Thompson discovered an elementary particle - electron. This discovery led to a quick explanation of how and why the metals conduct an electrical current. At the turn of the 20th century, Paul Drude created a theoretical model which tried to explain the electric conductivity of metals. Apart from this, it's application covers for example the description of dielectric resonances and the conductivity in dielectrics. These latter topics will be the focus of this chapter.

In systems with restoring force (i. e. polar lattice vibrations or movement of valence electrons) it is possible to describe the system's response to incident harmonically oscillating electromagnetic field $Ee^{i\omega t}$ via damped harmonic oscillator [26].

The resonant frequency ω_0 of the system is determined by the harmonic part of its potential.

The mathematical description is done via second order differential equation for the polarisation, which provides the permittivity of the material. The relative permittivity can be written as

$$\varepsilon_r = 1 + \frac{f}{\omega_0^2 - \omega^2 + i\omega\Gamma} \quad , \quad (1)$$

where ω is the angular frequency of incident light, Γ is the damping coefficient and f is an oscillator strength. As such, we have obtained a model for dielectric resonance with resonant frequency ω_0 .

Note that for the case of $\omega = 0$ we are talking about static permittivity ε_{stat} and for the case where ω is much larger than ω_0 we are talking about the infinite permittivity ε_∞ , which is equal to one in this model case.

In the case of interaction with phonon, this resonance can be

described as

$$\varepsilon_r = 1 + \frac{\omega_L^2 - \omega_0^2}{\omega_0^2 - \omega^2 + i\omega\Gamma} \quad , \quad (2)$$

where the f parameter was expressed in terms of the frequency of the longitudinal and transverse phonon, $\omega_L = \omega_0 \varepsilon_{stat}^{1/2}$ and ω_0 respectively.

Obviously in real materials we can have more than one resonance

$$\varepsilon_r = 1 + \sum_j \frac{f_j}{\omega_{0j}^2 - \omega^2 + i\omega\Gamma_j} \quad , \quad (3)$$

where index j denotes the different resonances.

In metals there is no restoring force acting upon free electrons. One finds

$$\varepsilon_M = 1 + \frac{\omega_p^2}{i\omega\Gamma - \omega^2} \quad . \quad (4)$$

When comparing equations (1) and (4) we can clearly see, that the expression (4) is analogous to (1) with $\omega_0 = 0$. The parameter ω_p is analogous to ω_L and it is called angular frequency of the plasma resonance, or just the plasma frequency. It characterizes longitudinal resonant oscillations of free charges and its value is important for the optical behaviour of a conductor.

1.2 Transfer matrix formalism and its relation to guided modes

Let us note, that all materials from here on will be considered to be non-magnetic, therefore the relative permeability is $\mu_r = 1$.

The transfer matrix formalism (TMF) is a tool for solving the behaviour of electromagnetic fields in a layered structure. A transfer matrix is introduced for each layer and it connects the tangential components of the fields at the two interfaces of the layer (e.g. E_{01}, H_{01} and E_{12}, H_{12} in figure 1).

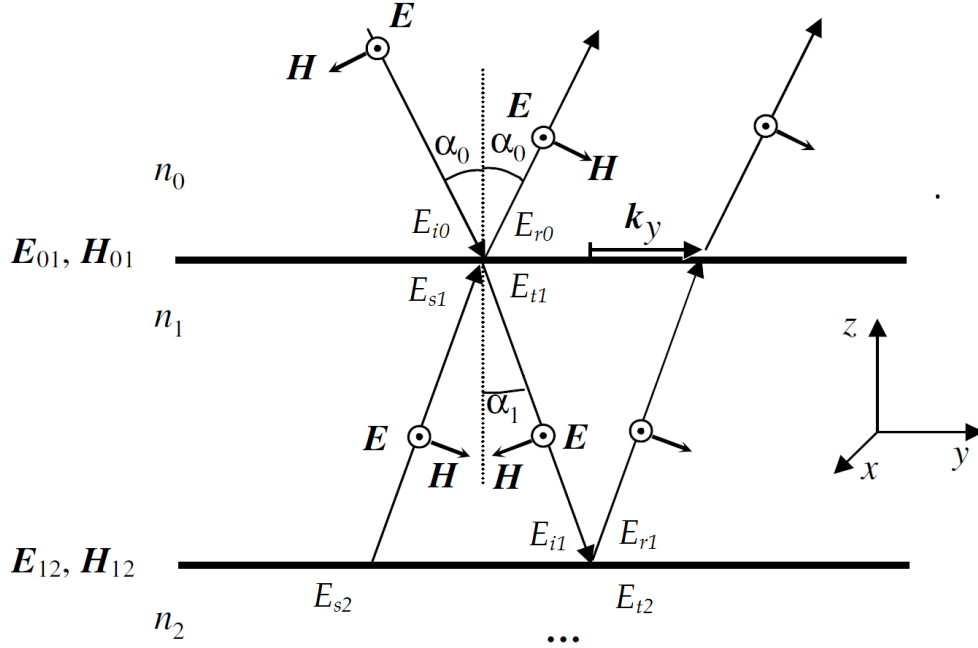


Figure 1: Definition of symbols and coordinate system for TMF TE polarization. Here, we have one layer with refractive index n_1 and superstrate and substrate with refractive indices n_0 and n_2 , respectively.

Let us consider a scheme depicted in figure 1. This example contains only a single layer n_1 with a substrate n_2 and superstrate n_0 , but it is valid for any layered structure in which the role of a substrate could be taken by another layer etc. In [27] it is proved that for both TE and TM polarization, the tangential fields can be related via the following expression

$$\begin{pmatrix} E_{01} \\ \eta_0 H_{01} \end{pmatrix} = \begin{pmatrix} \cos \delta_1 & \frac{i \sin \delta_1}{\gamma_1} \\ i \gamma_1 \sin \delta_1 & \cos \delta_1 \end{pmatrix} \begin{pmatrix} E_{12} \\ \eta_0 H_{12} \end{pmatrix}, \quad (5)$$

where η_0 is the vacuum wave impedance, $\delta_1 = \omega n_1 d_1 \cos \alpha_1 / c$ is the so

called phase factor due to the propagation of the wave inside the layer, where d_1 is the thickness of a layer and γ_1 takes the form

$$\gamma_1 = n_1 \cos \alpha_1 \quad \text{for TE and} \quad \gamma_1 = \frac{n_1}{\cos \alpha_1} \quad \text{for TM polarization.} \quad (6)$$

The cosine term can be defined for any layer as

$$\cos \alpha_j = \frac{\sqrt{k_j^2 - k_y^2}}{k_j}, \quad (7)$$

where α_j is the angle of incidence and k_j is the reflected wave.

Note, that if the k_j wave is evanescent in said layer or sub/superstrate, the equation (7) is still true. Obviously the cosine from equation (7) can be complex. In particular, for a medium without losses it is real or imaginary. If it is imaginary we are talking about guided modes since $k_y > k_j$ which is the characteristic property of guided modes.

Using figure 2 we can confirm the validity of the equation (7), and obtain relations for $\cos \alpha_0$ and $\cos \alpha_2$ as

$$\cos \alpha_0 = \frac{\sqrt{k_r^2 - k_y^2}}{k_r} = -i \frac{\sqrt{-k_r^2 + k_y^2}}{k_r}, \quad \cos \alpha_2 = -i \frac{\sqrt{-k_t^2 + k_y^2}}{k_t}. \quad (8)$$

Note the minus signs due to our convention ($e^{i\omega t}$).

We have made use of a fact, that cosines are obviously equal to $k_{j,z}/k_r$ and $k_{t,z}/k_t$ respectively and that the square of any vector in 2D space is equal to the sum of the squares of its components - therefore we used

$$\begin{aligned} k_{r,z}^2 &= k_r^2 - k_y^2 \\ k_{t,z}^2 &= k_t^2 - k_y^2 \end{aligned} \quad (9)$$

In general, a structure consisting of multiple layers, can be still described by a single transfer matrix M_{TOT} . We obtain this matrix as a product of all matrices of individual layers: $M_{TOT} = M_1 M_2 \dots M_N$, where

$$M_j = \begin{pmatrix} \cos \delta_j & \frac{i \sin \delta_j}{\gamma_j} \\ i \gamma_j \sin \delta_j & \cos \delta_j \end{pmatrix}, \quad j \in \{1, N\}. \quad (10)$$

Note that the δ_j and γ_j are defined analogously to equation (6) for the j -th layer of the structure and upper/bottom half-spaces as well.

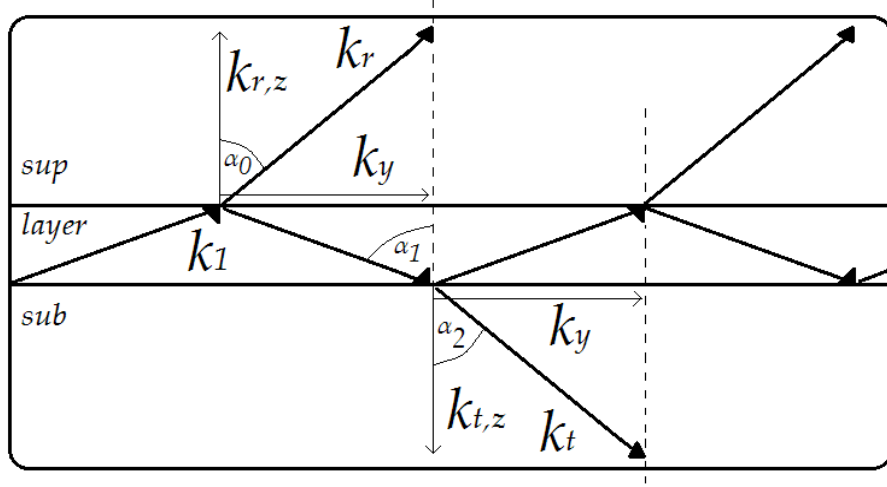


Figure 2: Scheme for cosine term derivation. One can easily see the relation between k_r and its components via cosine of α_0 . The same goes for k_t vector.

In figure 1 we have defined partial waves E_{il} , E_{sl} , E_{r1} and E_{t1} . These waves are connected by the following relations

$$\begin{aligned} E_{sl} &= E_{r1} e^{-i\delta} \\ E_{il} &= E_{t1} e^{-i\delta} \end{aligned} \quad (11)$$

Similar partial waves can be defined in any layer of the layered structure. In the case depicted in figure 1, we have only E_{i0} and E_{r0} in the superstrate and E_{s2} and E_{t2} in the substrate. We define a mode guided by the structure by an evanescent character of the fields in the upper and lower half-space, i.e. $E_{i0} = E_{s0} = 0$. Note that in this sense the SPP is considered as a guided wave, too.

Since k_y is constant in every layer (due to the Snell's law) and since it is real for guided waves, we will use it for the description of SPPs. The k_y represents the wave vector of guided wave and obviously the relation of $\omega(k_y)$ describes the dispersion of the guided mode, therefore giving us the knowledge of the guided mode behaviour.

Considering the above mentioned condition for evanescent waves $E_{i0} = E_{s2} = 0$ we obtain

$$\begin{aligned} E_{01} &= E_{r0} \\ E_{12} &= E_{t2} \end{aligned} \quad . \quad (12)$$

For a TE polarization, we also use

$$\begin{aligned} \eta_0 H_{01} &= -\gamma_0 E_{r0} \\ \eta_0 H_{12} &= \gamma_2 E_{t2} \end{aligned} \quad , \quad (13)$$

Equation (5) takes the form

$$\begin{pmatrix} E_{r0} \\ -\gamma_0 E_{r0} \end{pmatrix} = \begin{pmatrix} m_{11} & m_{12} \\ m_{21} & m_{22} \end{pmatrix} \begin{pmatrix} E_{t2} \\ \gamma_2 E_{t2} \end{pmatrix} \quad \text{for TE pol.} \quad (14)$$

Note that we have used a general form of the transfer matrix. This leads to a system of two equations described by matrix

$$\begin{pmatrix} m_{11} + \gamma_2 m_{22} & -1 \\ m_{21} + \gamma_2 m_{22} & \gamma_0 \end{pmatrix} \begin{pmatrix} 0 \\ 0 \end{pmatrix} \quad , \quad (15)$$

which has a non-trivial solution

$$m_{21} + \gamma_2 m_{22} + \gamma_0 m_{11} + \gamma_0 \gamma_2 m_{12} = 0 \quad . \quad (16)$$

For TM polarization the tangential fields are equal to $E_{01} = \eta_0 H_{r0} \gamma_0^{-1}$ and $E_{12} = \eta_0 H_{t0} \gamma_2^{-1}$. Introducing this into equation (5) gives us an analogy to equation (14)

$$\begin{pmatrix} H_{r0} / \gamma_0 \\ -H_{r0} \end{pmatrix} = \begin{pmatrix} m_{11} & m_{12} \\ m_{21} & m_{22} \end{pmatrix} \begin{pmatrix} H_{t2} / \gamma_2 \\ H_{t2} \end{pmatrix} \quad , \quad (17)$$

which again leads to the same solution (16).

1.3 Conclusion

In this chapter we have derived a general condition for the propagation of a guided mode (16) inside any planar structure. This condition describes every guided mode for both TE and TM polarisation, including SPP.

We have also stated, that the k_y vector serves as a wave vector of such a guided mode, while relation $\omega(k_y)$ serves as a dispersion curve of such a mode.

Since this gives us a complete description of SPP, in the following chapter we will solve this condition for different scenarios in which an SPP can propagate.

2. Surface plasmon polariton calculation via TMF

2.1 Metal/isotropic dielectric interface

In this paragraph we show simple derivation of the SPP propagation condition along the metal/isotropic dielectric interface by means of TMF i.e. equation for guided modes (16). We only need to realize that the transfer matrix (10), in case of SPP propagating along a metal/isotropic dielectric interface, is identity matrix. It is true because formally, the layer from figure 1 has a zero thickness in this case. Condition (16) is therefore simplified to

$$\gamma_0 = -\gamma_2 \quad , \quad (18)$$

where these gamma factors are defined analogously to equation (6).

To solve equation (18) for TM polarisation we introduce cosine terms from equation (7) and we obtain

$$-n_0^2 \sqrt{k_y^2 - \frac{\omega^2 n_2^2}{c^2}} = n_2^2 \sqrt{k_y^2 - \frac{\omega^2 n_0^2}{c^2}} \quad . \quad (19)$$

Note that this equation is a solution for TM polarization. For TE polarisation, one could obtain a similar equation to equation (19), however, in case of TE polarisation it has no non-trivial solution. Equation (19) can be solved for k_y as

$$k_y^2 = \frac{\omega^2}{c^2} \frac{n_0^2 n_2^2}{n_0^2 + n_2^2} \quad . \quad (20)$$

Note, that equation (19) can only be solved, if one of the refractive indices is purely imaginary and other real. Such a behaviour of i.e. medium 0 can be found in dielectrics in the stop-bands and in medium 2 in metals below plasma frequency. Therefore we can conclude that an SPP propagating along a single interface requires the interface to be between a dielectric and a metal.

The surface plasmon can propagate in two distinct regimes. First

regime is when the frequency of the SPP is small (orders of magnitude smaller than the plasma frequency). This in turn means that the absolute value of the refraction index of the metal is much larger than refraction index of the superstrate

$$|n_2| \gg n_0 \quad . \quad (21)$$

Note that the condition (21) refers explicitly to the studied THz range (where the negative permittivity is conveyed by the ordinary metal).

Equation (20) therefore gets simplified into the form of

$$k_y^2 \approx \frac{\omega^2}{c^2} n_0^2 \quad , \quad (22)$$

meaning, that in the Zenneck regime the dispersion curve is nearly linear, very close to (but still below) the light line of the dielectric superstrate and proportional to the refraction index of the superstrate. Moreover, the penetration depth in the Zenneck regime is very high in the dielectric material. It can be even substantially longer than the SPP's wavelength (which, in itself is very long; e.g. the electromagnetic wave at 1 THz has a wavelength of $300\mu\text{m}$). On the other hand, the penetration depth in the metal is extremely small, therefore the Zenneck waves can propagate over very long distances without a significant loss.

The second regime is obtained for

$$n_2 \approx -i n_0 \quad . \quad (23)$$

This regime is characterised by a flat dispersion:

$$\omega = \frac{\omega_p}{\sqrt{n_0^2 + 1}} \quad , \quad (24)$$

and the SPP's frequency reaches the same order of magnitude as the plasma frequency. Also, the penetration depth into the superstrate in this regime is smaller than SPP's wavelength.

Based on the above, one can conclude that the Zenneck regime is clearly more appropriate for the purposes of the spectroscopy, since it is

defined by the refraction index of the superstrate, and the penetration depth into it is high.

2.2 Metal/anisotropic dielectric interface

In the previous section, we have considered the superstrate to be isotropic dielectric. Now we will look at more general example, where the superstrate is now anisotropic dielectric.

This case is important since our goal is to study anisotropic materials and therefore the knowledge of SPPs behaviour propagating along such an interface is crucial.

We consider this dielectric to have uni-axial anisotropy with extraordinary axis perpendicular to the interface (along the z axis in figure 1), therefore it is isotropic along the x - y plane (and obviously along all the planes parallel to x - y plane). This geometry is very important to some experimental situations encountered in THz spectroscopy.

To find an analogical counterpart to equation (20) we need first to develop a TMF for anisotropic medium.

2.2.1 TMF for the anisotropic medium

Our goal is to obtain the condition for SPP propagation along the metal/anisotropic interface. It can be done using the continuity of tangential components of evanescent electric and magnetic fields similar to (12) and (13).

For the case of TM polarization, based on the figure 2, we obtain the following for the k_r and k_t wave vectors

$$\begin{aligned} k_r &= \frac{n_{0a}\omega}{c} (0, \sin \alpha_0, \cos \alpha_0) \\ k_t &= \frac{n_2\omega}{c} (0, \sin \alpha_2, -\cos \alpha_2) \end{aligned} \quad , \quad (25)$$

where n_{0a} is the refraction index of the wave in anisotropic medium for the given angle α_0 .

Using $\mathbf{k} \cdot \mathbf{D} = 0$ one obtains the displacement field of

$$\begin{aligned} D_r &= D_r(0, -\cos \alpha_0, \sin \alpha_0) \\ D_t &= D_t(0, \cos \alpha_2, \sin \alpha_2) \end{aligned} \quad , \quad (26)$$

where D_r and D_t are the amplitudes.

We can now obtain the electric field based on the relation $\mathbf{D} = \epsilon \cdot \mathbf{E}$ as

$$\begin{aligned} E_r &= D_r \left(0, \frac{-\cos \alpha_0}{\epsilon_{\parallel}}, \frac{\sin \alpha_0}{\epsilon_{\perp}} \right) \\ E_t &= \frac{D_t}{\epsilon_2} (0, \cos \alpha_2, \sin \alpha_2) \end{aligned} \quad . \quad (27)$$

Next, we can obtain the magnetic field using maxwell equation $\text{rot } \mathbf{E} = \partial \mathbf{B} / \partial t$. The magnetic field then can be calculated using

$$\mathbf{H} = \frac{\mathbf{k} \times \mathbf{E}}{\omega \mu_0} \quad . \quad (28)$$

The conditions of continuity of tangential components of the evanescent electric and magnetic fields then lead to the following equation:

$$\frac{n_{\parallel}^2}{n_{0a} \cos \alpha_0} = \frac{n_2}{\cos \alpha_2} \quad , \quad (29)$$

where $n_{\parallel} = (\epsilon_{\parallel})^{1/2}$. The equation (29) has the meaning of a condition for propagation of SPP along metal/anisotropic dielectric interface. It is formally analogical to equation (18), and its right-hand side has the meaning of γ_{2r} , therefore

$$\frac{n_{\parallel}^2}{n_{0a} \cos \alpha_0} \equiv \gamma_{0a} \quad . \quad (30)$$

In equation (30) we have defined anisotropic counterpart to isotropic gamma factor from TMF in chapter 1.2.

One can also easily show that in our geometry the transfer matrix reads:

$$M_{ja} = \begin{pmatrix} \cos \delta_{ja} & \frac{i \sin \delta_{ja}}{\gamma_{ja}} \\ i \gamma_{ja} \sin \delta_{ja} & \cos \delta_{ja} \end{pmatrix} \quad , \quad (31)$$

where γ_{ja} is defined analogously to (30) and the phase factor now takes the form of $\delta_{ja} = \omega n_{ja} d_j \cos \alpha_j / c$ where n_{ja} is the anisotropic index of refraction of the j -th layer.

For n_{0a} we write

$$\frac{1}{n_{0a}^2} = \frac{\sin^2 \alpha_0}{n_{\perp}} + \frac{1 - \sin^2 \alpha_0}{n_{\parallel}} = \sin^2 \alpha_0 \left(\frac{1}{n_{\perp}} - \frac{1}{n_{\parallel}} \right) + \frac{1}{n_{\parallel}^2} . \quad (32)$$

$$n_{0a} = n_{\parallel}^2 \left[1 - \frac{k_y^2 c^2}{\omega^2} \left(\frac{1}{n_{\perp}} - \frac{1}{n_{\parallel}} \right) \right]$$

We can rewrite the $\cos \alpha_0$ from equation (7) as

$$\cos \alpha_0 = \frac{\sqrt{n_{0a}^2 - \frac{c^2 k_y^2}{\omega^2}}}{n_{0a}} , \quad (33)$$

And consequently, using equation (32) we can write

$$n_{0a} \cos \alpha_0 = \sqrt{n_{0a}^2 - \frac{c^2 k_y^2}{\omega^2}} = \sqrt{n_{\parallel}^2 - \frac{c^2 k_y^2}{\omega^2} \frac{n_{\parallel}^2}{n_{\perp}^2}} = n_{\parallel} \cos \alpha_{\perp} , \quad (34)$$

where

$$\cos \alpha_{\perp} = \frac{\sqrt{n_{\perp}^2 - \frac{c^2 k_y^2}{\omega^2}}}{n_{\perp}} . \quad (35)$$

In conclusion, in this chapter, we have inferred the transfer matrix formalism for TM polarisation for an anisotropic uni-axial medium, with an optical axis perpendicular to the interface, using the continuity of the tangential fields. We have also derived the condition for the propagation of SPP along metal/anisotropic dielectric interface (29).

2.2.2. Solution of the condition (29)

After introducing cosine factors from equation (7) into equation (29), one obtains

$$-n_{\parallel}^2 \sqrt{k_y^2 - \frac{\omega^2 n_{\parallel}^2}{c^2}} = n_{\perp}^2 \sqrt{k_y^2 - \frac{\omega^2 n_{0a}^2}{c^2}} , \quad (36)$$

and then, after introducing anisotropic refraction index from equation (32) we can solve equation (36) as

$$\frac{k_y^2 c^2}{\omega^2} = X = \frac{\epsilon_M \epsilon_G}{\epsilon_M + \epsilon_G} \frac{\epsilon_A \epsilon_M - \epsilon_G}{\epsilon_M - \epsilon_G} , \quad (37)$$

where ϵ_M is permittivity of a metal, $\epsilon_G = (\epsilon_{\parallel} \epsilon_{\perp})^{1/2}$ and $\epsilon_A = (\epsilon_{\perp} / \epsilon_{\parallel})^{1/2}$ and the X can be understood as the square of the effective refraction index of the plasmon. Note that if there is no anisotropy, that is when $\epsilon_{\parallel} = \epsilon_{\perp}$, we get the same equation as equation (20).

Let us discuss this result. In the Zenneck regime, that is for low frequencies (orders of magnitude lower than plasma frequency) one finds

$$|\epsilon_{\perp}| \gg \epsilon_G \rightarrow X \approx \epsilon_A \epsilon_G = \epsilon_{\perp} , \quad (38)$$

Thus in this regime, we find that the dispersion of the plasmon depends solely on ϵ_{\perp} i. e. on the out-of-plane component of the permittivity. The polarisation of the plasmon is then perpendicular to the interface. On the other hand in the saturated regime, the permittivity of the metal approaches the value of $-\epsilon_G$ and therefore

$$X \approx \sqrt{\epsilon_{\perp} \epsilon_{\parallel}} , \quad (39)$$

meaning that the polarisation of the SPP will be close to circular. We can therefore conclude that in the scenario where the SPP propagates along metal/anisotropic dielectric interface, in order to only measure the out-of-plane permittivity, we need to be in the Zenneck regime of the propagation.

2.3 SPP in an isotropic dielectric layer deposited on a metallic surface

In order to perform the spectroscopy of thin films using SPP we need to understand the behaviour of SPP propagating along metal/dielectric thin film interface, with isotropic superstrate above this film.

To obtain the condition for propagation in this case, we again use equation (16), with now non zero transfer matrix in form of (10). One finds

$$\begin{pmatrix} H_{r0}/\gamma_0 \\ -H_{r0} \end{pmatrix} = \begin{pmatrix} \cos \delta_1 & \frac{i \sin \delta_1}{\gamma_1} \\ i \gamma_1 \sin \delta_1 & \cos \delta_1 \end{pmatrix} \begin{pmatrix} H_{t2}/\gamma_2 \\ H_{t2} \end{pmatrix} . \quad (40)$$

As a result we will obtain a condition for SPP propagation in a single dielectric layer

$$(\gamma_2 + \gamma_0) \cos \delta_1 - i \left(\frac{\gamma_0 \gamma_2}{\gamma_1} + \gamma_1 \right) \sin \delta_1 = 0 , \quad (41)$$

where index 0 belongs to superstrate, 1 belongs to the layer and 2 belongs to the substrate.

2.4 SPP in an anisotropic dielectric layer deposited on a metallic surface

In this case, we will work in the same manner as in previous chapter, however we need to take the anisotropy of the film into the account. In chapter 2.2.1 we have shown how the γ_0 factor changes due to the anisotropy of the material it is connected to. Similarly to this, now the factors γ_1 and δ_1 of the anisotropic film will change, since they are connected to anisotropic layer

$$\delta_1 \equiv \delta_{1a} = \frac{\omega}{c} n_{\parallel} d_1 \cos \alpha_{\perp} \quad , \quad (42)$$

$$\gamma_1 \equiv \gamma_{1a} = \frac{n_{\parallel}}{\cos \alpha_{\perp}} \quad . \quad (43)$$

Obviously, formally the condition is the same as in equation (41), however we need to substitute for γ_1 and δ_1 in accordance to equations (42) and (43). the guided modes (14) are then given by the following condition

$$(\gamma_2 + \gamma_0) \cos \delta_{1a} - i \left(\frac{\gamma_0 \gamma_2}{\gamma_{1p}} + \gamma_{1p} \right) \sin \delta_{1a} = 0 \quad , \quad (44)$$

Note that the medium 0 is isotropic.

2.5 Solution of condition (41) and (44).

Fortunately the conditions for propagation of SPP along metal/thin film interface can still be solved analytically. We will solve only equation (44) however, since solution for (41) can be obtained from it, by placing $n_{\parallel} = n_{\perp}$.

In the following part, we will use the component of the permittivity tensor instead of ordinary and extraordinary refraction indices ($\varepsilon_{\parallel} = n_{\parallel}^2$, $\varepsilon_{\perp} = n_{\perp}^2$).

We begin by dividing eq. (44) by $\cos\delta_{1p}$ and we obtain

$$\tanh \Delta_{1p} = \frac{\mathcal{Y}_2 + \mathcal{Y}_0}{1 + \frac{\mathcal{Y}_2 \mathcal{Y}_0}{\mathcal{Y}_{1p} \mathcal{Y}_{1p}}} , \quad (45)$$

where $\Delta_{1p} = i\delta_{1p}$. In order to introduce dimensionless quantities relative to the plasma frequency it is convenient to define the substitutions from equation (46). Since the SPP's behaviour is scaled by the plasma frequency we obtain the same dispersion curves regardless of the metal's properties (plasma frequency). We define

$$\begin{aligned} K &= \frac{k_y c}{\omega_p} \\ \Omega &= \frac{\omega}{\omega_p} \\ D &= d \frac{\omega_p}{c} \end{aligned} . \quad (46)$$

$$X = \frac{k_y^2 c^2}{\omega^2} = \frac{K^2}{\Omega^2}$$

Note that the X has once again meaning of the square of effective refraction index.

Substituting equations (46) into eq. (45) we get

$$\tanh \left[\sqrt{\frac{\varepsilon_{\parallel}}{\varepsilon_{\perp}}} \Omega D \sqrt{X - \varepsilon_{\perp}} \right] = \frac{\frac{\varepsilon_2}{\sqrt{\varepsilon_{\parallel} \varepsilon_{\perp}}} \sqrt{\frac{X - \varepsilon_{\perp}}{X - \varepsilon_2}} + \frac{\varepsilon_0}{\sqrt{\varepsilon_{\parallel} \varepsilon_{\perp}}} \sqrt{\frac{X - \varepsilon_{\perp}}{X - \varepsilon_0}}}{1 + \frac{\varepsilon_2}{\sqrt{\varepsilon_{\parallel} \varepsilon_{\perp}}} \sqrt{\frac{X - \varepsilon_{\perp}}{X - \varepsilon_2}} \frac{\varepsilon_0}{\sqrt{\varepsilon_{\parallel} \varepsilon_{\perp}}} \sqrt{\frac{X - \varepsilon_{\perp}}{X - \varepsilon_0}}} , \quad (47)$$

which in terms of K (from equation (46)) takes the form

$$\tanh \left[\sqrt{\frac{\varepsilon_{\parallel}}{\varepsilon_{\perp}}} D \sqrt{K^2 - \varepsilon_{\perp} \Omega^2} \right] - \frac{\frac{\varepsilon_2}{\sqrt{\varepsilon_{\parallel} \varepsilon_{\perp}}} \sqrt{K^2 - \varepsilon_{\perp} \Omega^2} + \frac{\varepsilon_0}{\sqrt{\varepsilon_{\parallel} \varepsilon_{\perp}}} \sqrt{K^2 - \varepsilon_{\perp} \Omega^2}}{1 + \frac{\varepsilon_0 \varepsilon_2}{\varepsilon_{\parallel} \varepsilon_{\perp}} \sqrt{K^2 - \varepsilon_{\perp} \Omega^2} \sqrt{K^2 - \varepsilon_{\perp} \Omega^2}} = 0 \quad . \quad (48)$$

Note the importance of ε_{\perp} for the behaviour of the plasmon. The condition $X < \varepsilon_{\perp}$ or $X > \varepsilon_{\perp}$ changes the sign of the argument of the square roots, and consequently, it changes the character of the solution (surface plasmon vs. guided mode in the film). We also point out, that ε_{\parallel} does not have such an important role.

Equation (48) completely describes the propagation of surface plasmon along the thin layer and metallic substrate interface. Note that it describes the guided modes in dielectric film as well. They can be distinguished from the surface plasmon by the character of their dispersion curve (as it will be shown later) or by the form of the electric field inside the layer.

Relation $X(\Omega)$ gives us the dispersion curve of the SPP in this scenario, however equations (48) and (44) need to be solved numerically. In the following chapter we will discuss the character of the solution.

2.6. Conclusion

In this chapter, we have derived the conditions for SPP propagation along several different interfaces and we have also developed TMF for anisotropic medium.

Moreover we have discussed, that the SPP can only exist on the interface between metal and dielectric and we have defined two distinct regimes of propagation.

First, in Zenneck regime, when the SPP frequency is in order of THz, the plasmon has high penetration depth into the superstrate and the dispersion curve is linear, proportional to the index of refraction of the superstrate. Second, in the saturated regime, when the frequency of the SPP is comparable to plasma frequency, the dispersion curve saturates at the frequency with value of $\omega = \omega_p/(\epsilon_0 + 1)^{1/2}$, while the penetration depth into the superstrate is small (note that ϵ_0 is the permittivity of the superstrate, as usual).

In case of the metal/anisotropic dielectric interface, we have also discussed that the polarisation of the SPP in Zenneck regime is perpendicular to the interface, while in the saturated regime it is circular.

Based on all of the above, we can conclude, that for the purposes of the SPP spectroscopy, we need to be in the Zenneck regime of propagation, that is in THz frequency range.

3. Graphical representation of theoretical research

In chapter 2, we have derived equations which describe the behaviour of SPP propagating along various interfaces. In this chapter we will focus on graphical representation of said formulas, and explain SPP's behaviour in detail.

3.1 Metal/isotropic dielectric interface

We begin with the simplest case of metal/isotropic dielectric interface, described by equation (20).

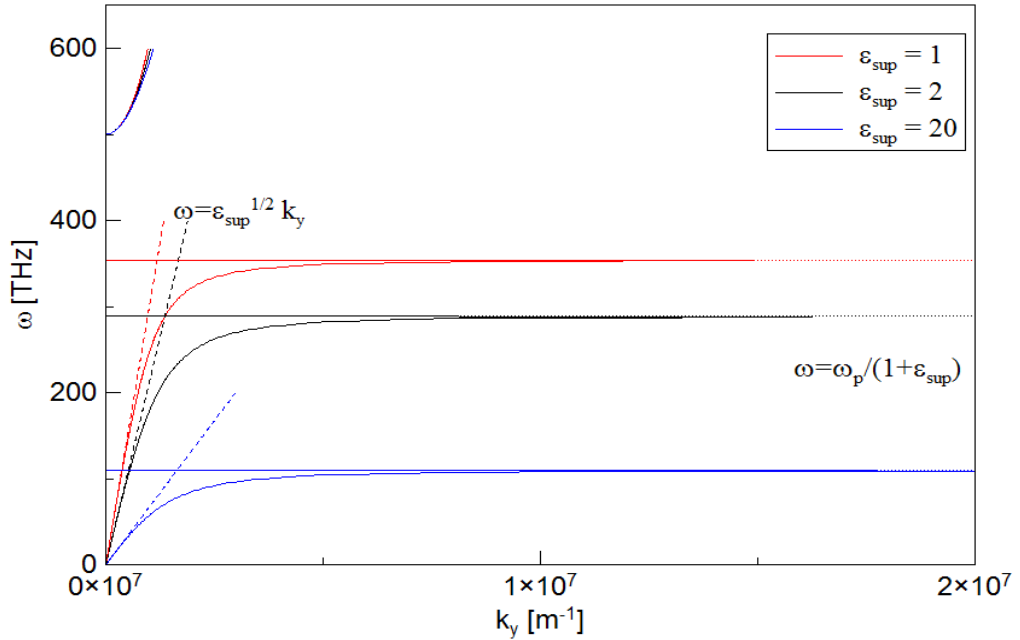


Figure 3: Dispersion curves for the metal/isotropic dielectric interface. Plasma frequency $\omega_p = 500$ THz, permittivity of the dielectric superstrate can be seen in the legend in the top right corner, no damping. We can see two specific regimes in which the SPP propagates – at low frequencies (bottom-left part of the plot) we see the so called Zenneck regime in which the dispersion curve is approximately a linear curve proportional to the square root of the permittivity of the superstrate (dashed line). At higher frequencies we observe the saturated regime where the dispersion is almost flat and the curve tends to a limit value (dotted line) described as $\omega_p / (1 + \epsilon_{\text{sup}})$, where „sup,, describes superstrate.

In figure 3 we have introduced two distinct regimes in which a SPP can propagate – the Zenneck regime and a saturated regime, discussed in chapter 2.

We can see that the behaviour of the Zenneck regime can be altered by changing the permittivity of the superstrate. Another way with which we can achieve the same result is obviously to lower the plasma frequency. This can be done by creating a sub-wavelength decoration (or grating) on the surface of metal. The effective permittivity of the metal is then lowered and the plasma frequency in turn lowers as well. In such case we talk about a so called spoof plasmon [19].

So far, we have discussed the case of a lossless metal. In the following figure we will see a case with non-zero damping coefficient (eq. (4)):

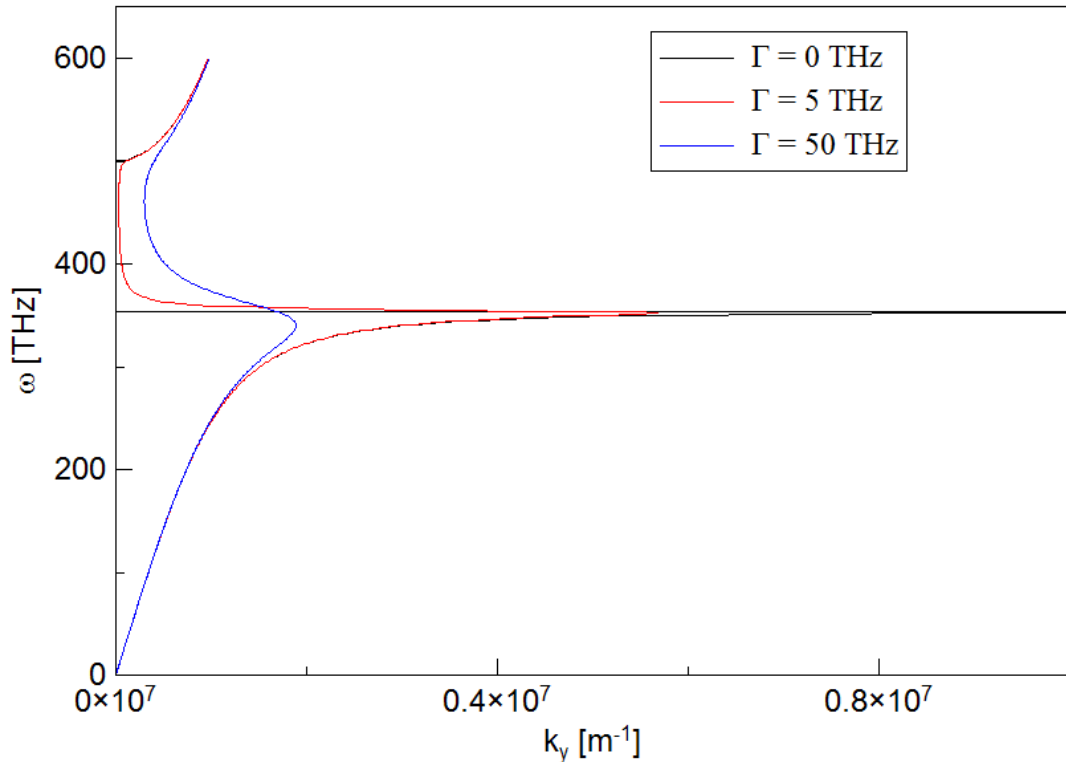


Figure 4: Dispersion curves for the metal/isotropic dielectric interface. Plasma frequency $\omega_p = 500\text{THz}$, superstrate permittivity $\epsilon_{sup} = \epsilon_0 = 1$, damping intensity can be seen in the legend. The saturated regime disappears, however Zenneck regime is weakly affected as well – the propagation of SPP is somewhat more attenuated.

While it would seem, that in figure 4 only the saturated regime is affected by damping, it is important to note, that the SPP's attenuation length in the direction of k_y vector gets smaller with metal's higher damping as well. The SPP is simply attenuated and can not propagate without losses, because of the damping in the metal.

From these figures it is clear, that we can modulate both Zenneck regime and saturated regime to our needs just by changing the permittivity of the superstrate or lowering the plasma frequency.

3.2. Metal/anisotropic dielectric interface

Next we will talk about anisotropic superstrate as opposed to the isotropic one in the previous chapter.

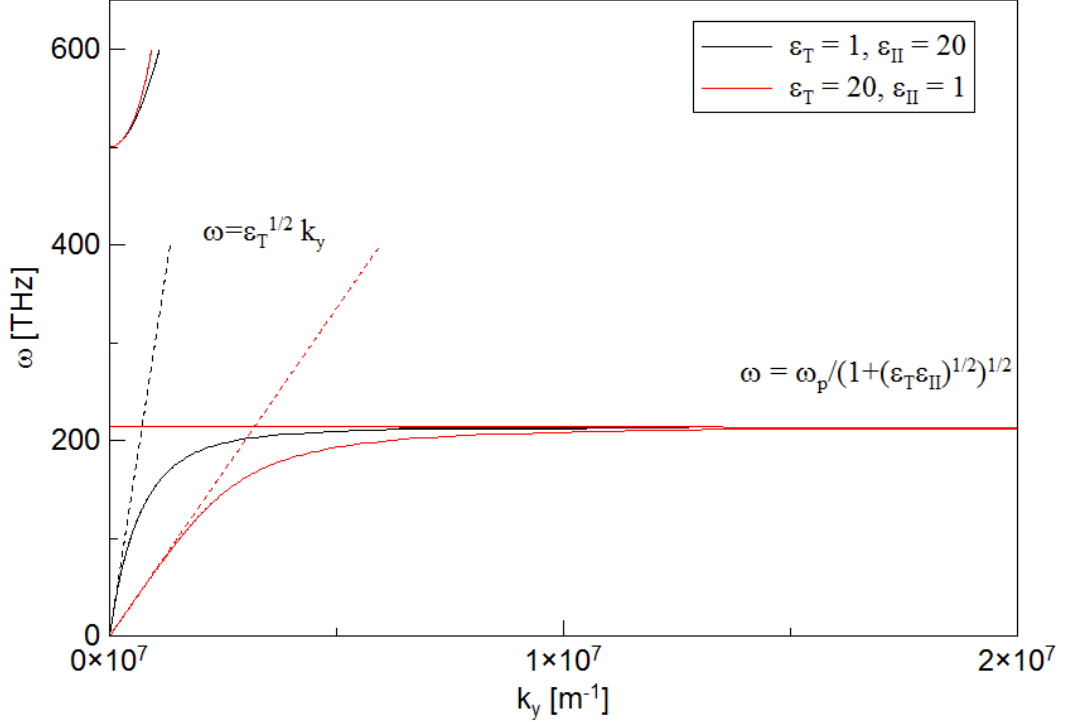


Figure 5: Dispersion curves for metal/anisotropic dielectric interface. Plasma frequency $\omega_p = 500$ THz, no damping. We have opted for two distinct cases of perpendicular and parallel permittivities provided in the legend. As discussed in chapter 2, the saturated regime limit depends merely on product of ϵ_{\parallel} and ϵ_{\perp} , consequently, the saturated frequency of the surface plasmon is the same for both plotted cases. The Zenneck regime only depends on the perpendicular permittivity however. Note, that index „T,, represents perpendicular while „II,, represent parallel permittivity.

In figure 6 we will show dispersion curves with a non zero damping coefficient in the permittivity of the metal. More importantly however, the perpendicular permittivity will not be a constant value. It will exhibit a dispersion described by a harmonic oscillator (1). This feature may represent a polar phonon mode in the dielectric material, for example.

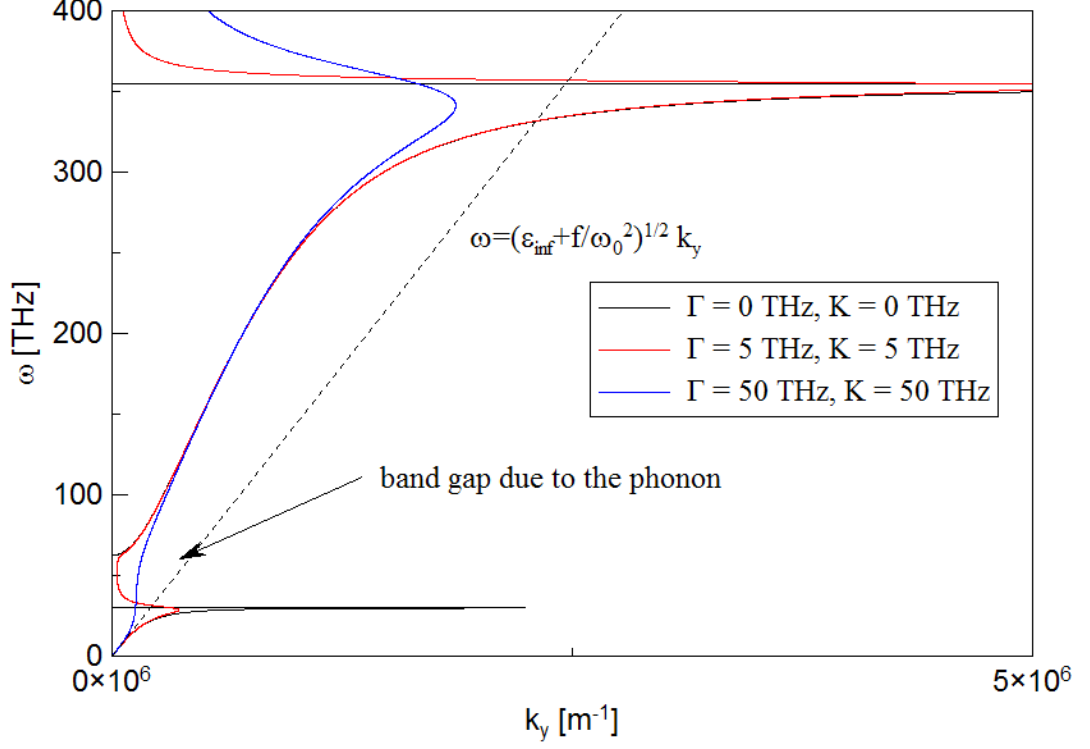


Figure 6: Dispersion curves for metal/anisotropic dielectric interface with a dispersion of the out-of-plane constant ε_{\perp} of the dielectric. Plasma frequency $\omega_p = 500\text{THz}$, the damping intensity of the dielectric Γ and of the metal K can be seen in the legend. The out-of-plane permittivity is given by equation (1) with $\omega_0 = 30\text{THz}$, the in-plane permittivity is equal to 1. We see a formation of a new, narrower, band gap at around 50THz. Close to the phonon resonance, more precisely in the reststrahlen band of the phonon, where both the permittivity of the metal and of the dielectric are negative, the plasmon can not propagate. Position of the gap is tied to the ω_0 and it is at this point that the gap opens. The width of the gap depends on the oscillator strength f (or in other word, on the longitudinal phonon frequency. The f was set be 3.10^{27} Hz^2 in this model). The linear part near zero can be described as $\omega = (\varepsilon_{inf} + f/\omega_0^2)^{1/2} k_y$. Note that the $\varepsilon_{inf} = \varepsilon_{\infty}$ from chapter 1.

As seen in figure 6, an anisotropic superstrate gives us the opportunity to change the behaviour of the Zenneck regime, without changing the properties of the saturated regime. Phonon like resonance in permittivity translates into a band gap in the dispersion curve. Above the band gap, the permittivity of ε_{\perp} is lowered by f/ω_0^2 as the phonon mode does not contribute to the permittivity at these higher frequencies. This sets a new Zenneck regime with a reduced slope of the SPP dispersion curve. Also note,

that a resonance in ϵ_{\parallel} in the Zenneck regime of the plasmon would not lead to any significant additional dispersion (band gap) of the SPP, as ϵ_{\parallel} contributes to the plasmon behaviour only in the saturated regime.

3.3. SPP in a dielectric layer

The last scenario we have discussed in chapter 2 was a SPP propagating along metal/thin layer interface. In this case, it is not possible to derive an explicit solution in the form of $k=k(\omega)$ therefore we proceed using numerical calculations of equation (48), which governs both isotropic and anisotropic cases. The result is obtained by evaluating the left hand side of function (48) for all combinations of reduced wave vectors K and frequencies Ω and looking for the function value equal to zero. Our graphs represent a colour-map picture of the logarithm of the left-hand-side of equation (48), where the green (or yellow) colour represents a positive or slightly negative logarithm value, while dark colours (blue and black) represent large negative logarithm values, i. e. a close neighbourhood of the solution of (48). Dark colour then indicates states on the dispersion curve of an allowed mode (either surface plasmon or a guided mode) of the layered structure. In every graph in this chapter, the y-axis denotes Ω and x-axis denotes K .

3.3.1. isotropic layer

First, let us have a look on a situation when we have „deposited,, a rather thick layer, $D = \omega_p d/c = 33,36$. Where the d is the real thickness of the layer. Note that for plasma frequency of 500THz, $d = 20000nm$. In the following graphs, if referred to the thickness of the layer, the real value d is meant. Also, in all cases the superstrate is vacuum therefore its permittivity is 1.

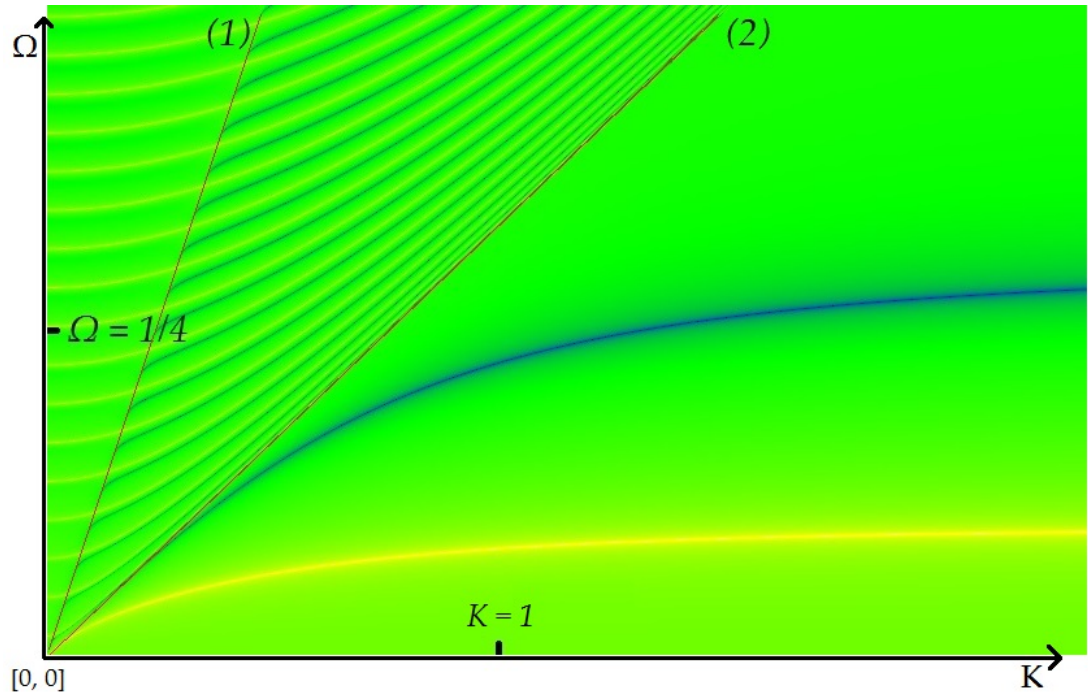


Figure 7: SPP propagating along metal/thick isotropic dielectric layer with a permittivity of 10. $D = 33,36$, corresponding to $d = 20000nm$ for the plasma frequency $\omega_p = 500THz$, no damping. The surface plasmon mode can be observed below the line denoted as (2). We observe similar behaviour to that shown in figure 3. (1) and (2) are the light lines corresponding to the superstrate (surrounding dielectric) and film, respectively. One can see several modes in the space delimited by (1) and (2). These modes are guided by the film but do not have the plasmonic character - see the discussion in chapter 2.5.

In figure 7 we have shown the light lines (1) and (2). They play an analogous role to the Zenneck regime asymptotes seen in figure 3. The line (1) is determined by the permittivity of the superstrate ϵ_0 as $\Omega = K/\epsilon_0$, while

the line (2) is determined by the permittivity of the layer ϵ_1 as $\Omega = K/\epsilon_1$.

The space between these two lines may be populated by the modes guided in the film: the wave vectors of the waves below the light line (1) can not be accepted as propagating waves in the superstrate while the modes above the line (2) can still possess a real wave vector in the film.

Since in case of figure 7 the Zenneck regime is dominated by the permittivity of the layer, we can conclude, that the superstrate above the layer has no effect. This means that the layer is sufficiently thick to acts as a bulk dielectric.

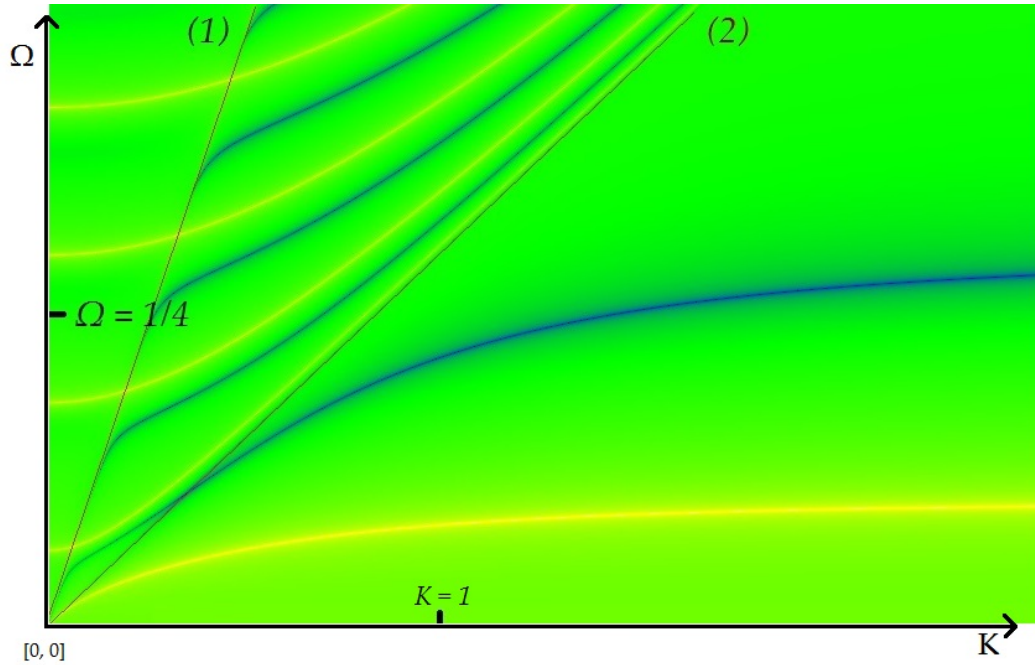


Figure 8: SPP propagating along metal/isotropic dielectric layer with a permittivity of 10. $D = 8,34$, corresponding to $d = 5000nm$ for the plasma frequency $\omega_p = 500THz$, no damping. The light lines of the superstrate (1) and film (2) are defined similarly as in figure 7. Note that for this thickness, the Zenneck regime does not approach limit (2) but it approaches limit (1) close to the origin.

In figure 8 we see, that for thinner layers the Zenneck regime is split. Near the origin, the solution is dominated by the permittivity of the superstrate. This is because in the long-wavelength limit the film thickness is very small compared to the de-localization of the plasmon in the z-direction.

The influence of the film on the plasmon properties is therefore only minor. The second regime can be found at slightly higher frequency where the surface plasmon dispersion curve intersects the light line of the film (2). Here we are still very close to the Zenneck regime and the role of the film in the plasmon dispersion becomes dominant. For $K > 2$ the curve begins to saturate.

Let us move to even thinner layer's width.

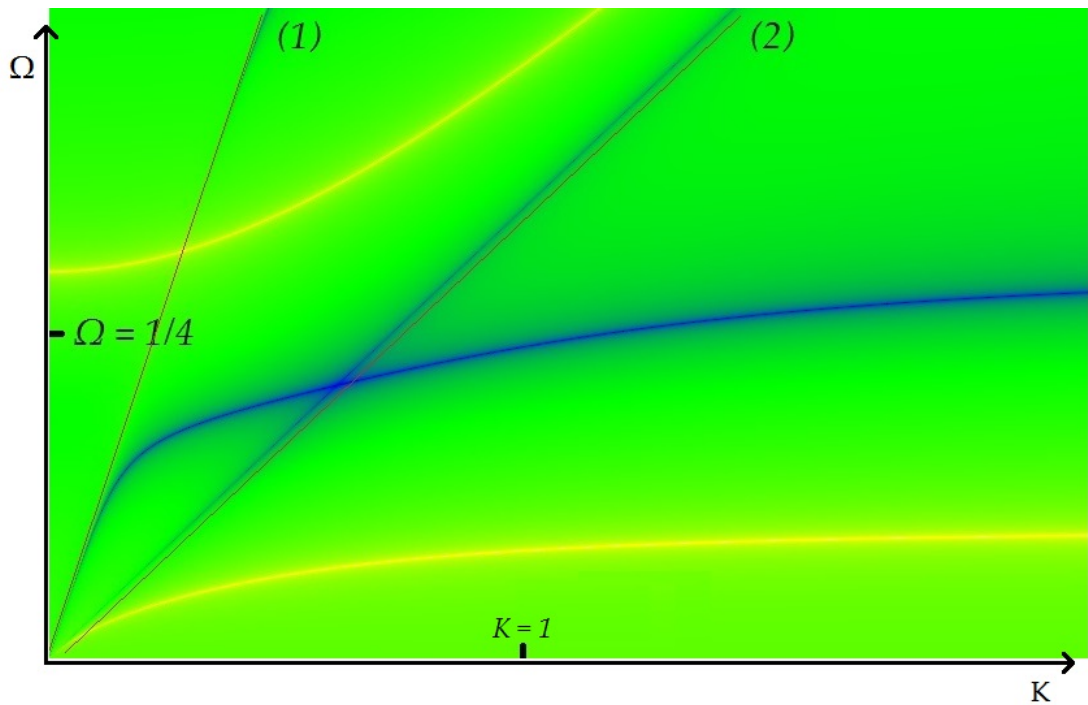


Figure 9: SPP propagating along metal/isotropic dielectric layer with a permittivity of 10. $D = 1,67$, corresponding to $d = 1000nm$ for the plasma frequency $\omega_p = 500THz$, no damping. We have noted the limit values (1) and (2) in the same manner than in figure 7. Note that we have offset the limit (2) so a new line could be seen – it will be discussed below this figure.

In figure 9, we can see that for this thickness, the Zenneck regime gets dominated by the permittivity of the superstrate even more. At the point of crossing of the line (2) we now can not say that we are still in the Zenneck regime, since the curve begins to saturate.

Note that we have moved the limit (2) line slightly to the right in this figure, so we could reveal the new blue line. The line has been present in all

the figures in chapter 3.3, however it has been covered by limit (2) line. The blue line represents singular solution originating in the intersection of the SPP dispersion curve and limit (2), It is not a true solution of the dispersion curve and it is to be disregarded in this manner.

Let us have a look on the last example, where we will use a rather thin layer with thickness $d = 100nm$.

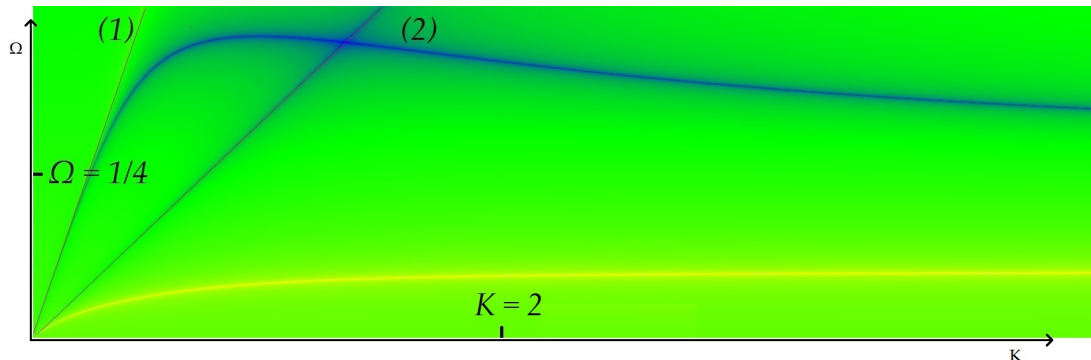


Figure 10: SPP propagating along metal/isotropic dielectric layer with a permittivity of 10. $D = 0,17$, corresponding to $d = 100nm$ for the plasma frequency $\omega_p = 500THz$, no damping. We have noted the limit values (1) and (2) in the same manner than in figure 7. The Zenneck regime is now strongly pinned to the light line (1). Permittivity of the layer can not be accessed in the Zenneck regime now. Note the change of scale in x-axis.

In conclusion, we have discussed the character of the solution in the case of SPP propagation along metal/thin film dielectric interface for different thicknesses of the layer. We have found out, that in order to access the permittivity of the layer with the Zenneck regime, we need to use rather thick layers, since as it can be seen in figure 10, for thin layers, the dispersion curve in Zenneck regime gets dominated by the permittivity of the superstrate.

3.3.2. anisotropic layer

Lastly we will discuss the case of anisotropic layer.

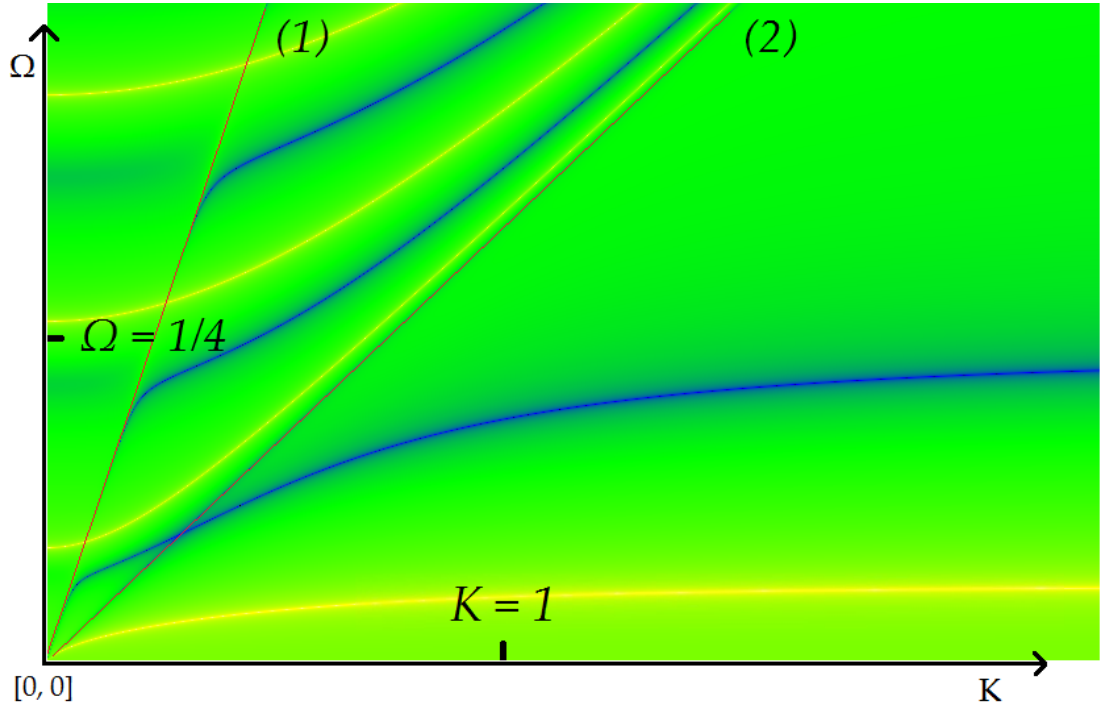


Figure 11: SPP propagating along metal/anisotropic dielectric layer with a permittivities $\epsilon_{\parallel} = 30$, $\epsilon_{\perp} = 10$. $D = 3,34$, corresponding to $d = 2000nm$ for the plasma frequency $\omega_p = 500THz$, no damping. (1) and (2) are the light lines corresponding to the superstrate (surrounding dielectric) and film, respectively.

In figure 11 we can see two light lines, similarly as before. The line (1) is determined by the permittivity of the superstrate ϵ_0 as $\Omega = K/\epsilon_0$, on the other hand, line (2) is now determined only by the perpendicular permittivity of the layer ϵ_{\perp} as $\Omega = K/\epsilon_{\perp}$. This becomes obvious, if we interchange the perpendicular and parallel permittivities same, as in case of figure 5 into $\epsilon_{\parallel} = 10$, $\epsilon_{\perp} = 30$.

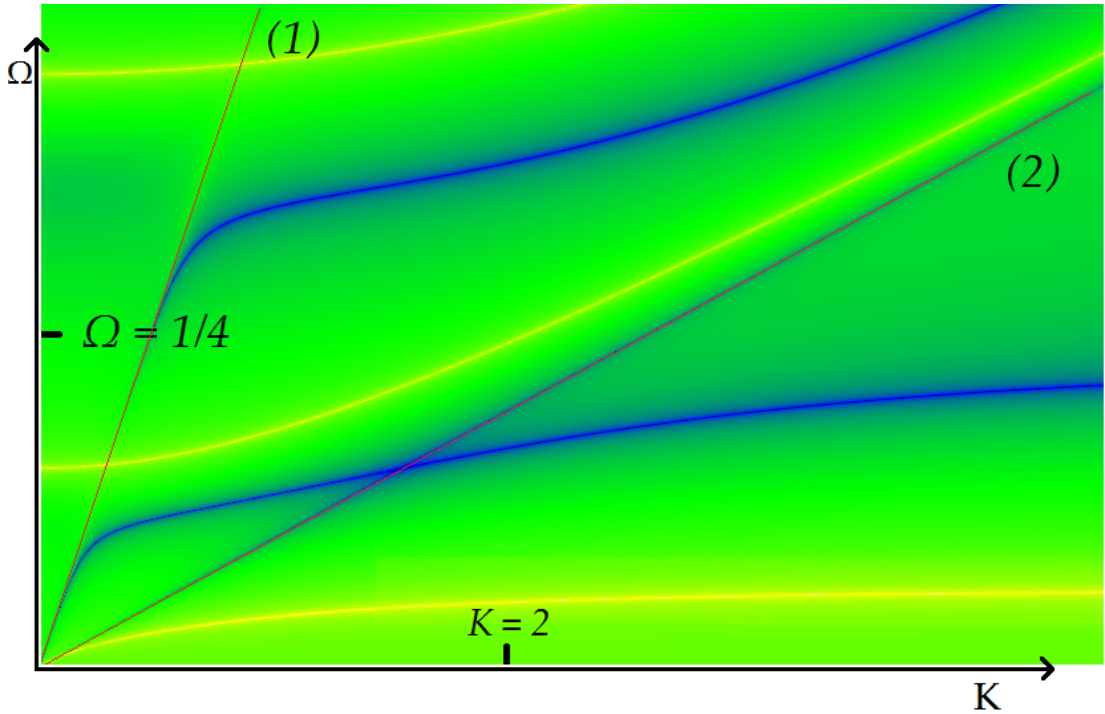


Figure 12: SPP propagating along metal/anisotropic dielectric layer with a permittivities $\epsilon_{\parallel} = 10$, $\epsilon_{\perp} = 30$. $D = 3,34$, corresponding to $d = 2000nm$ for the plasma frequency $\omega_p = 500THz$, no damping. (1) and (2) are the light lines corresponding to the superstrate (surrounding dielectric) and film, respectively.

If we were to compare figures 11 and 12 side by side, we would find out, that just as in the case of figure 5, the limit of the saturated regime is unchanged if the value of permittivities is interchanged. On the other hand, we can see, that since line (2) is determined as $\Omega = K/\epsilon_{\perp}$ it is more tilted to the right, as one would expect. The beginning of the Zenneck regime is dominated by the permittivity of the superstrate in both cases however.

We can therefore conclude, that the behaviour of the SPP propagating along metal/anisotropic interface, is similar to the case of figure 5 in a sense, that the saturated limit is defined by a product of ϵ_{\perp} and ϵ_{\parallel} , and that the light line (2) is now only defined by perpendicular permittivity.

3.4. Conclusion

In this chapter we have described analytical solutions for different scenarios of SPP propagation graphically. We have also confirmed some theoretical predictions on the shape of the dispersion curves made in chapter 2.

We now know, that the Zenneck regime in case of simple interface between metal/isotropic depends solely on permittivity of the superstrate and plasma frequency. Similarly, in case of metal/anisotropic dielectric, the Zenneck regime depends only on perpendicular permittivity of dielectric (and plasma frequency).

In case of interface between metal and layer, we have found out that thicker layers are preferable since for thin layers we do not have access to layer's permittivity by itself.

Lastly, we have described the behaviour of the phonon like resonance in permittivity via harmonic oscillator (equation (1)) and we have found out, that the presence of such a resonance translates into the band gap in the dispersion curve.

4. Numerical solution of SPP propagation

Until now, we based our analysis on analytically derived equations. However, even for a simple structure consisting of a dielectric layer on top of a metallic substrate, the solution gets complicated rather quickly, as seen in (48). Obviously the TMF allows us to work with even more than one such layer, but then even greater complexity of the obtained solutions is to be expected in such a case (depending on the layer thickness, birefringence and permittivity values).

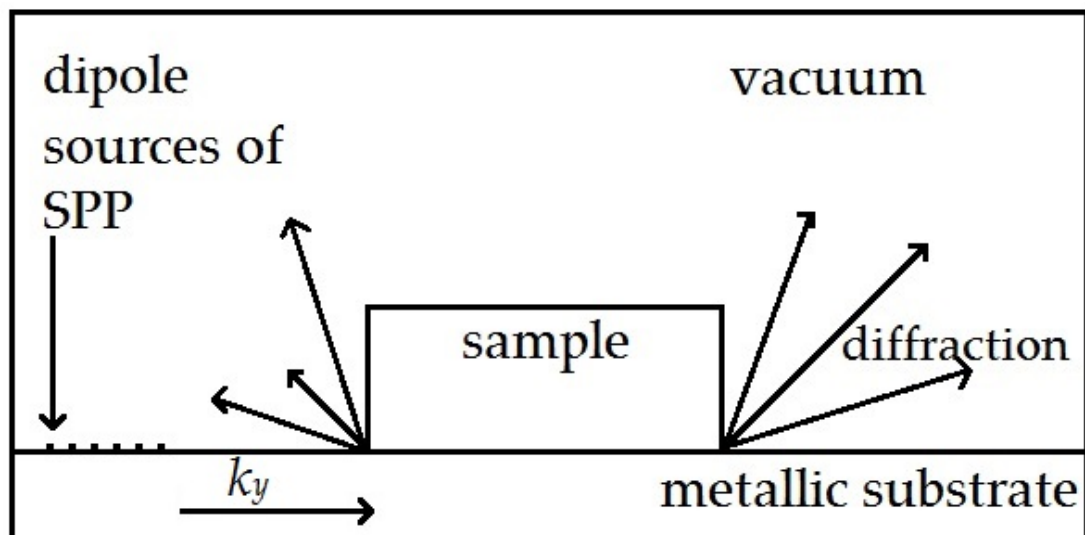


Figure 13: Scheme of the simulated experiment. We have a dielectric sample placed on top of a metallic substrate. On the left we can see an array of electric dipoles which generates our surface wave (see chapter 4.2.) in the direction of k_y . When the SPP enters the sample, we expect it to diffract as depicted by arrows left of the sample. We expect a similar effect to occur when SPP leaves the sample. The rest of the space is vacuum.

In real measurements we are working with a small sample with finite dimensions, not with an infinite layer. The scheme of a typical experiment (and of the geometry that we consider in numerical simulations) is shown in figure 13. The surface plasmon is typically launched at a vacuum/metal interface. Experimentally one should position a broadband coupler on top of the metal which couples a freely propagating THz pulse into the surface

plasmon. In the simulations we may create for example a suitable dipole array to excite the surface plasmon at a specific frequency (specific point on its dispersion curve).

The plasmon then needs to be in-coupled/out-coupled at the input/output edge of the sample. At this point an edge diffraction is expected to occur due to the conditions of continuity of the fields near the edge. Such diffraction produces additional losses of the plasmon and this interaction may also lead to a phase change of the plasmon wave.

The amplitude and phase of the plasmon transmitted through the sample can be measured by the THz spectroscopy. We therefore performed numerical simulations in order to learn more about these interactions. Namely we ask (1) about the phase change of the plasmon wave due to the propagation in the sample and (2) whether some formula analogous, at least to some extent, to Fresnel equations for plane waves could be inferred also for the behaviour of the surface plasmons near the interface vacuum/sample.

For these reasons it would be very difficult, if not impossible, to obtain analytical description of a said measurement and as said it is feasible to look into different possibilities of description, which modern computer science offers, such as numerical solving.

For these purposes we used a software tool Comsol. Our foremost goal was to find out, if and how we can excite the SPP in Comsol since it offers several options as how to create a plane wave or a dipole directly, but offers none options as how to create a surface wave directly – see chapter 4.2.

4.1. The basics

According to [28] Comsol uses finite element method to do the calculations, therefore our first goal was to create the simulation in way that takes the least amount of computing power, and other computer resources (such as RAM space) to solve. This goes hand in hand with the number of degrees of freedom (DoF). The less we have, the lesser are the demands on a computer, and computing time.

For this reason, we performed the simulations in 2D: since our problem is invariant with respect to any translation along x axis (figure 1) we can reduce the problem to two dimensions (y-z plane).

Secondly, in order to reduce DoF we need not to over-mesh. Typically, in wave related simulation the recommended base value of the mesh size is $1/5$ of the wavelength. Obviously, this number varies, but based on our results seen later in this chapter, we believe, that our mesh was adequate.

Lastly, in order to keep the computing time short, we kept the simulated space as small as possible – typically the dimensions of the simulated model were within 10λ by 100λ , where λ is wavelength of the SPP.

4.2. Generating the wave

As previously mentioned, Comsol, can not generate the SPP directly in the emw. module (electromagnetic waves module) that we used. One can however use a point source define as an electric dipole. Our first attempt to generate the SPP was by using a single harmonically oscillating dipole and a slit. This meant, that we conducted the simulations in frequency domain, meaning that the frequency of emitted light was constant. Every model was therefore made for a series of frequencies.

SPP generation via the dipole and a slit can be seen in figure 14.

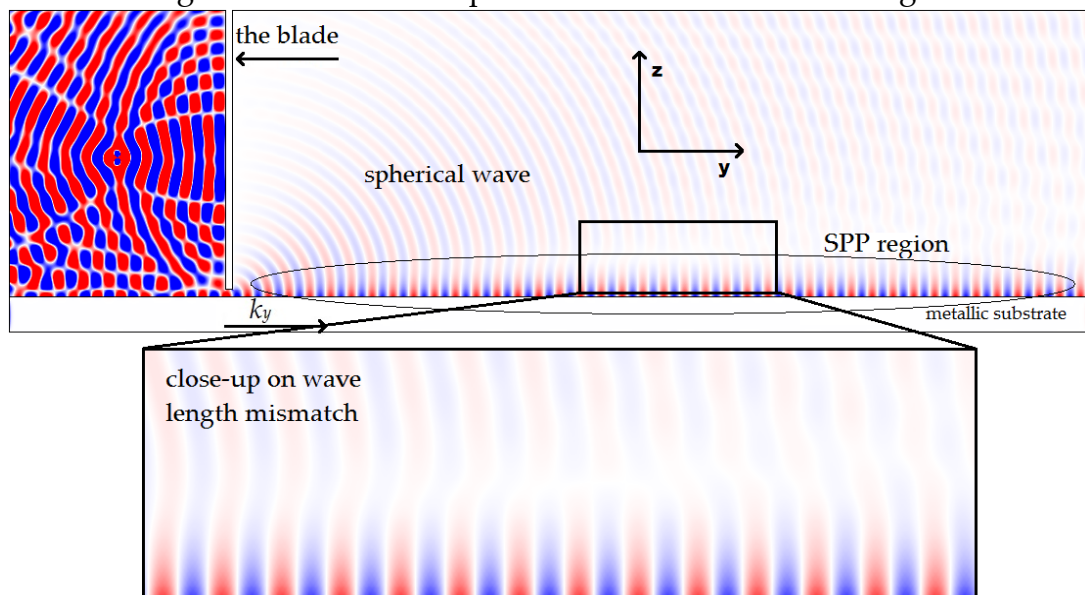


Figure 14: Simulation of launching the surface plasmon by using a single point dipole and a slit. The blade leaves a thin open space close to the metal surface allowing the plasmon to be excited. The distribution of the field is shown for the frequency 1 THz. Plasma frequency of the metal was set to 4THz.

Note the region of SPP is marked by an ellipse in figure 14. Also, the close-up clearly shows the difference in wavelength of the SPP and freely propagating spherical wave.

As stated above, in figure 14 we have opted for a plasma frequency of the metal at 4THz (similar plasma frequencies can be achieved, for example in a narrow band semiconductor like *InAs*). It is because we want to

point out the difference between the Zenneck regime and the saturated regime in the simulations. We consider the fact that for plasma frequency of 500THz the saturated regime is roughly at $\omega = 350 \text{ THz}$, while the Zenneck regime is roughly at $\omega = 1-10\text{THz}$, meaning that there is an order of magnitude difference in the wavelength between these two regimes. Consequently, this would translate into an order of magnitude different mesh size for both cases and therefore the computation time in the short wavelength case would be orders of magnitude higher.

The wavelength mismatch observed in the close-up part of figure 14 demonstrates that two distinct waves propagate close to the surface at the given frequency. The mode with shorter wavelength remains pinned to the surface and it corresponds to a wave with the wave vector outside the light cone. It unambiguously means that we observe the surface plasmon.

In order to get rid of the spherical wave we need to only select waves with certain k_y -vector, and the pinhole obviously does not provide the means to achieve that.

Our idea was to use several dipoles arranged in a linear array at (or close to) the interface of the substrate and superstrate - see figure 15. Their distance and the de-phasing of their oscillations may be selected in a manner to discriminate the wave vectors. See the figure 16 for results.

The dipoles in the array possess a specific relationship of the oscillation phase. The phase delay δ of the j -th dipole with respect to the first one is given by

$$\delta = \exp(-i k j \Delta) \quad , \quad (49)$$

where the k is k -vector for a particular frequency generated, calculated using the dispersion curve for a SPP (20), the j is an integer which denotes the dipole, and $\Delta = 50 \mu\text{m}$ is the distance between two adjacent dipoles.

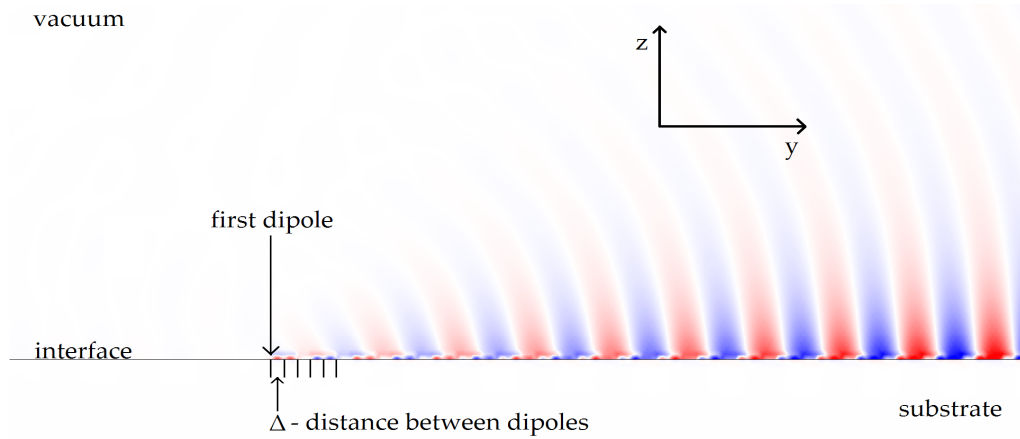


Figure 15: Source of a surface plasmon: array of de-phased electric dipoles positioned right in the interface. First dipole is denoted. Positions of the first few dipoles are marked by short vertical lines in the metal (right of the first dipole). Distance between dipoles is denoted as Δ . Dipole array continues till the right end of the picture (total amount of 60 dipoles). Frequency of the dipoles is 1 THz. E_z component of the electric field is shown.

The dipoles are oriented perpendicularly to the interface, so that their radiation pattern peaks in the y -direction. The plasmon wave can be efficiently generated owing to the constructive interference of partial waves emitted by individual dipoles. At the same time freely propagating wave will be dramatically reduced due to the destructive interference.

In figure 16 we can see the results of this new approach.

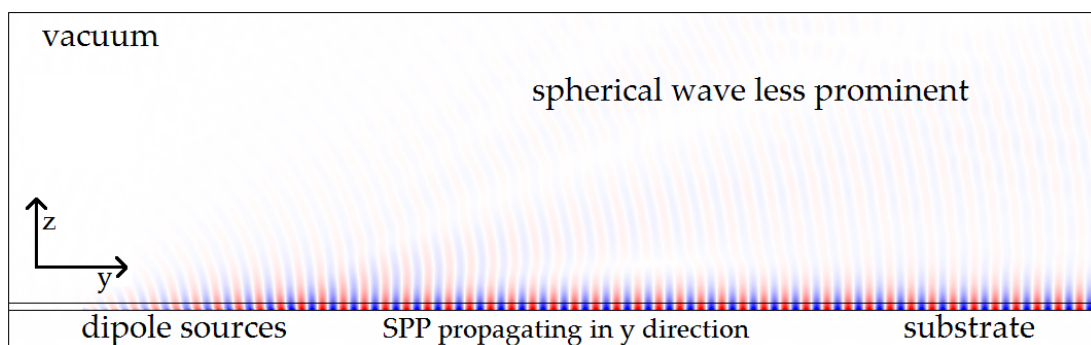


Figure 16: SPP generated by an array of dipoles. The dipole array source lies directly on the metal in the bottom left part of the simulation space. Frequency $\omega = 1THz$. The spherical wave from figure 14 is suppressed, while the efficiency of the SPP generation is increased. E_z component of the electric field is shown.

This new method of SPP generation clearly offers higher contrast between spherical wave amplitude and SPP amplitude. While in the first type of generation, the best contrast ratio (measured at the right-hand-side of the simulation space in figure 14) is 1:9 (spherical wave amplitude : SPP amplitude), the worst contrast ratio just behind the pinhole is 1:7. On the other hand the worst contrast ratio in the second type of generation is 1:21 with the best of 1:40, therefore we can conclude that this new method is clearly better for SPP generation.

Note that we measured the maximum of the amplitude of the SPP just above the interface. Also note, that while near the dipole array, the maximum of the SPP's amplitude increases with y-direction, however it saturates after the last dipole. We used this saturated value of the amplitude of SPP to calculate the aforementioned contrast ratios.

4.3. Results

Based on the figure 16 we have created a simulation using the SPP excitation method as described in chapter 4.2. In this simulation we have placed a 2mm wide sample with permittivity of 10 right on top of the metallic substrate. Our goal is to obtain the amplitude of the SPP as a function of y coordinate. Comparing this function to the similar function obtained from a simulation without a sample gives us the means to obtain a transmission coefficient of the sample and phase delay caused by the propagation of SPP inside the sample. The simulation's parameters are summed up in table 1.

Substrate rel. permittivity	From lossless Drude model, $\omega_p = 4\text{THz}$
Superstrate rel. permittivity	1
Sample rel. permittivity	10
Rel. permeability of all materials	1
Dipole frequency	0,5 – 1,2 THz, with step 0,05THz

Table 1: Material parameters used for SPP simulation in figure 17.

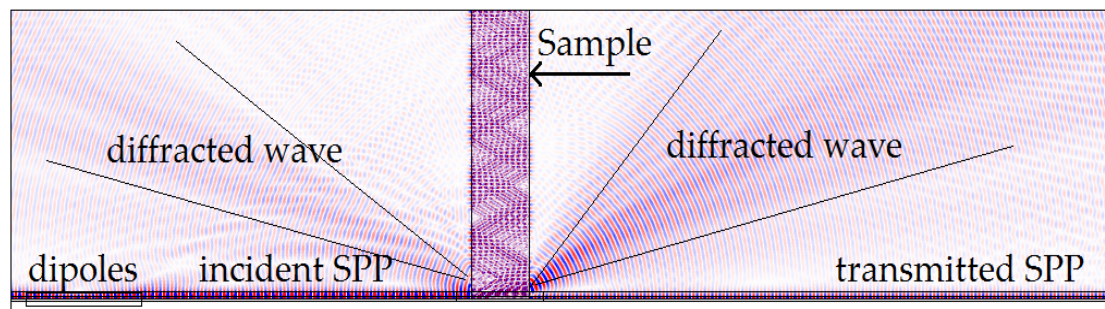


Figure 17: Result of the simulation for the SPP frequency of 1.1THz. In the middle there is a 2mm wide sample with permittivity of 10, placed on the metallic substrate. As previously, in the bottom left, there are electric dipoles generating incident SPP, which then passes through the sample and continues as transmitted SPP on the right of the sample. One can see diffracted waves left and right of the sample as expected in figure 13. E_z component of the electric field is shown.

A simulation of the propagation of SPP in the vicinity of a dielectric slab sample is shown in figure 17. We observe two waves coming from the bottom corners of the sample, this indicates radiative losses connected to SPP entering and leaving the sample.

In this geometry, the plasmon propagates along either metal/vacuum interface or metal/sample interface. For the sake of simplicity we will simply write that plasmon propagates in the vacuum or in the sample (even though we obviously mean propagation along the interface with metal).

The SPP is propagating from the left half-space (vacuum) to the dielectric sample in the middle. Because of the propagation through vacuum/sample interface SPP changed its character, since in dielectric it will be located in the different point on the dispersion curve, as seen in figure 18.

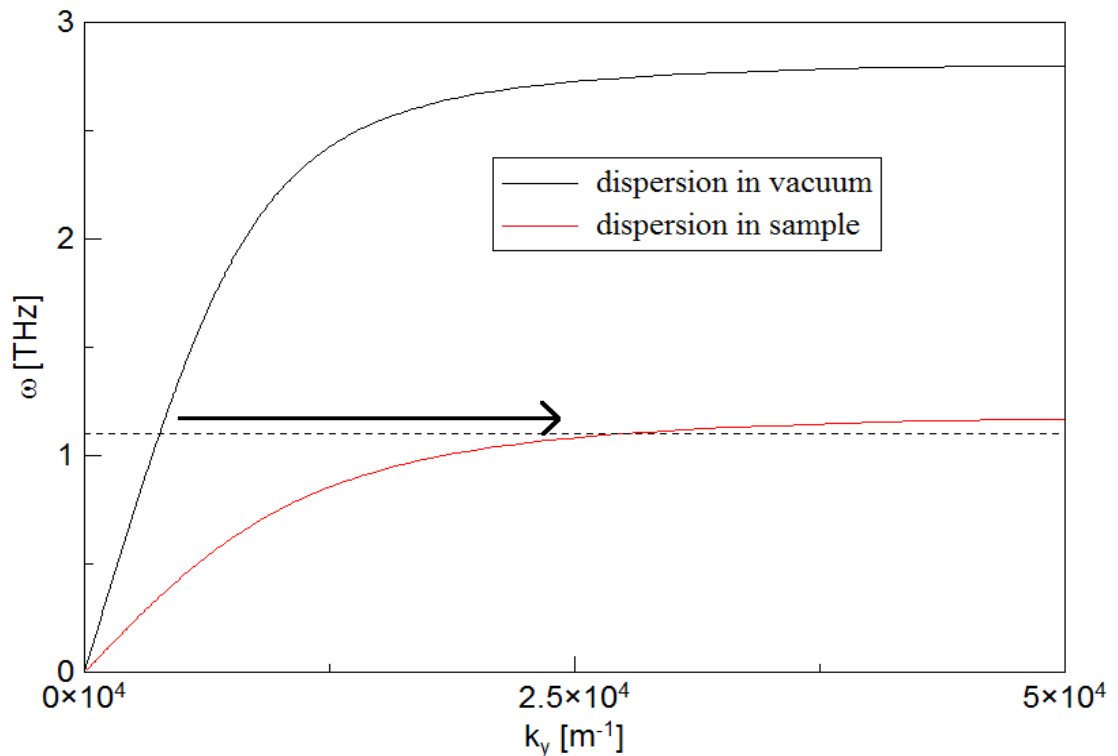


Figure 18: Comparison of dispersion curves for SPP propagation along metal/vacuum and metal/sample interfaces. Due to the difference between permittivities of the vacuum and of the sample, we can see, that at the frequency of 1.1THz (dashed line) the SPP is located in different points on the respective dispersion curves. The arrow denotes the transition from Zenneck regime in vacuum to almost saturated regime in the sample.

We expect, that the surface plasmon incident from vacuum onto the sample will be partially transmitted and partially reflected from the sample. Moreover the aforementioned radiative losses are present, as can be seen in figure 17.

The question is, if it is at all possible to find the description of SPP's transition through vacuum/sample interface, at least partially analogous to Fresnel equations, which describe the behaviour of the plane wave near such an interface.

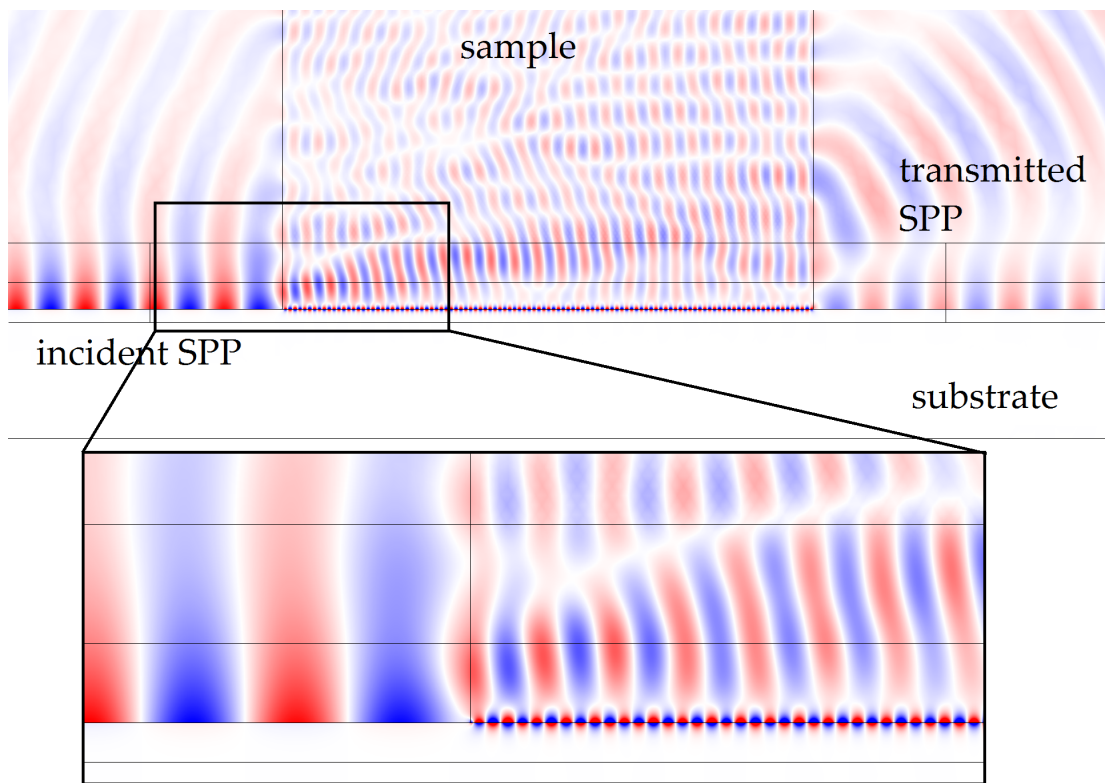


Figure 19: Closer view on incident and transmitted SPP at the sides of the sample. One can see faded out colours of the SPP behind the output face of the sample, meaning that the amplitude of depicted electric field E_z has lowered compared to incident SPP. Note the close-up of the bottom left corner of the sample, where the SPP is incident on the sample. Left of the sample, the SPP is still in Zenneck regime since the superstrate is vacuum with permittivity of one. Upon entering the sample we see a drastic shift in the wavelength of the SPP, meaning, that the SPP is no longer in Zenneck regime, since the permittivity of the superstrate (the sample) is 10.

Detail of the SPP propagation can be seen in figure 19. In this figure we clearly see the transition from the Zenneck regime in vacuum to saturated regime in the sample (we observe a dramatic confinement of the SPP in the z -direction as well as the dramatic shift in the SPP's wavelength as described in figure 18). Next the SPP propagates to the sample/vacuum interface. At this interface, part of the SPP is transmitted into the vacuum, while part is reflected back. Radiative losses also occur as well and the plasmon converts back to the Zenneck regime of propagation.

We evaluated the amplitude of the SPP's electric field just above the metal's surface in a line parallel with it.

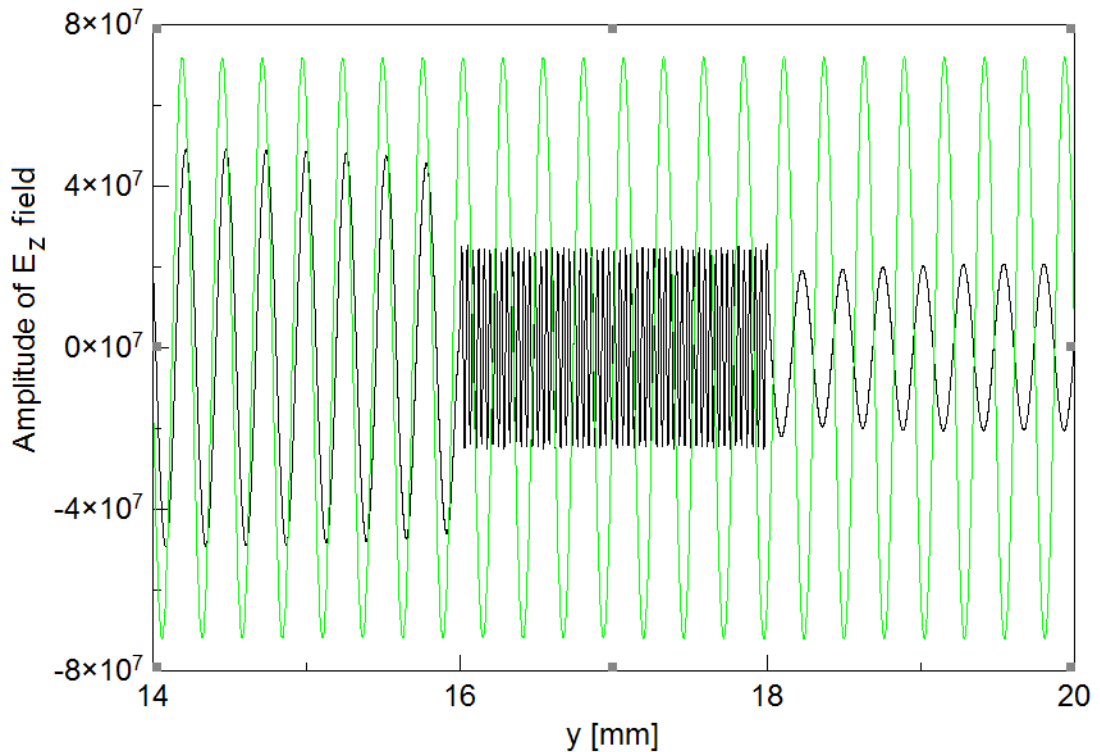


Figure 20: Variation of the E_z electric field component of the surface plasmon along the metal surface calculated in a Comsol simulation. In green we can see simulation without sample. In black we see a simulation with the sample. Data correspond to the simulation shown in figure 19. Note the dense oscillations of the black line in the middle, corresponding to SPP propagating in saturated regime inside the sample.

In figure 20 we can see a comparison of the amplitude of SPP when propagating in a simulation with/without a sample. In green, one can see the

oscillations of SPP's electric field in a simulation where no sample is present. Amplitude of these oscillations does not change in space. In black, we see oscillations obtained in the simulation with the sample. When SPP enters the sample, the amplitude of the oscillations is decreased and the frequency increases (corresponding to the shift from Zenneck to saturated regime). When the SPP leaves the sample, the amplitude of oscillations decreases even further. Lastly, note the decreased amplitude of the black curve in front of the sample due to the interference of incident and reflected wave.

A significant phase shift of the oscillations behind the sample compared to the reference ones can be seen. Hence, It is possible to deduce the phase shift of the transmitted wave from the simulation. Similarly, comparing amplitudes of the green and black curves, on the right-hand side of the sample will result in the transmission coefficient. In this manner, one can calculate the dependences of the phase shift and of the transmission amplitude on the frequency.

Proper description of the data comes from the fact, that the phase shift can be interpreted via the dispersion curve:

$$k_y = \frac{\Delta\varphi}{d} + \frac{2\pi f}{c} \sqrt{\frac{\varepsilon_0 \varepsilon_2}{\varepsilon_2 + \varepsilon_0}} \quad , \quad (50)$$

where ε_0 and ε_2 are the permittivities of the vacuum (since we are comparing the propagation through the sample with propagation through vacuum) and of the metal respectively, f is a frequency in THz, and $\Delta\varphi$ is overall phase shift

$$\Delta\varphi = \varphi + 2\pi(m-n) \quad , \quad (51)$$

where $\varphi \in (0, 2\pi)$ is a phase shift obtained from the simulation by aligning the black maxima with adjacent green maxima behind the sample in figure 20, m is an integer describing the number of complete wavelengths in the 2mm wide sample, while n describes the number of complete

wavelengths in vacuum of the same width. Equation (50) has analytical counterpart

$$k_y = \frac{2\pi f}{c} \sqrt{\frac{\epsilon_0 \epsilon_2}{\epsilon_2 + \epsilon_0}} \quad (52)$$

where $\epsilon_0 = 10$ now has the meaning of the permittivity of the dielectric sample. Comparing equations (52) and (50) yields

$$\frac{2\pi f}{c} \sqrt{\frac{10\epsilon_2}{\epsilon_2 + 10}} = \frac{\Delta\varphi}{d} + \frac{2\pi f}{c} \sqrt{\frac{1\epsilon_2}{\epsilon_2 + 1}} \quad (53)$$

Equation (53) describes the comparison of analytically and numerically obtained phase shift for one frequency f . The results are shown in figure 21.

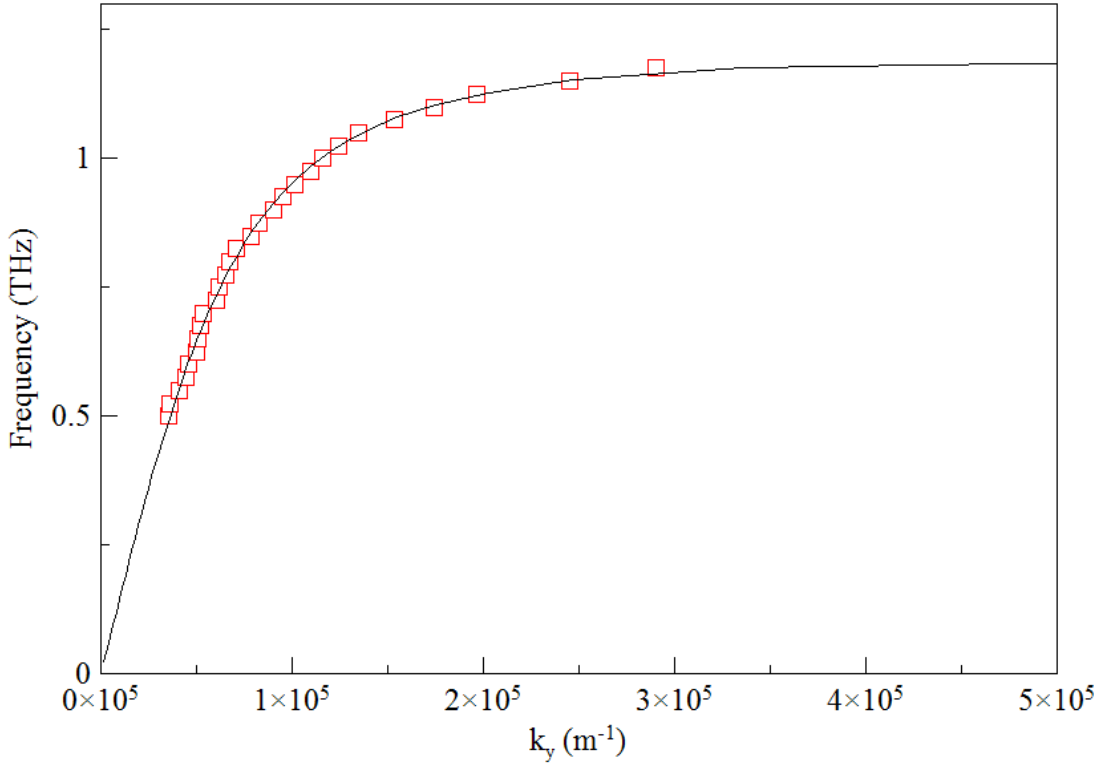


Figure 21: Comparison of theoretically obtained phase shift of the SPP due to the propagation inside the sample (black line) and numerically obtained data (red squares).

Note that due to the lack of time, we used approximation of equation (50): $k_y = \varphi + 2\pi m$ to obtain the points from the figure 21. However, we have used equation (50) to calculate several points from figure 21, such as for

frequencies 5,5; 0,7 and 0,9 THz. For these points the correlation with analytical predictions is very good, error is within few percent of the calculated value.

As for the transmission coefficient, it can be seen in figure 22. One can see, that the dependence exhibits peaks and dips, similar to airy function describing the transmission of dielectric slab by normally incident light.

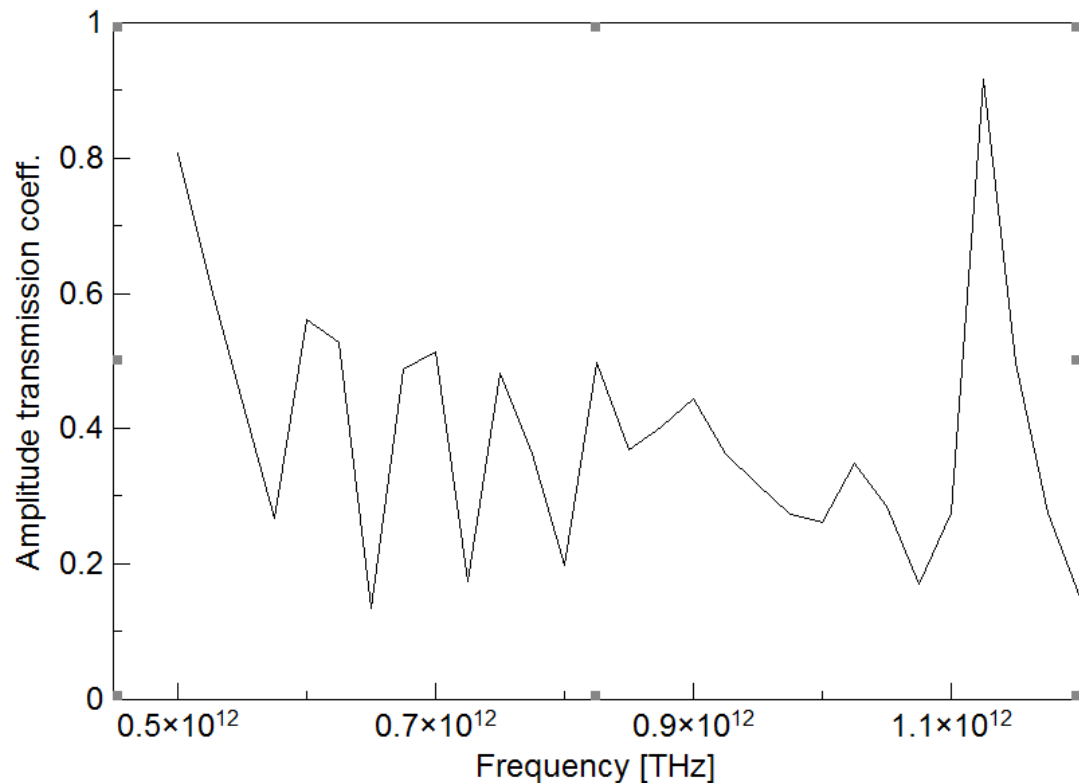


Figure 22: Transmission coefficient obtained from numerical simulation as comparison of the amplitude of transmitted SPP and amplitude of the SPP propagating through vacuum.

It is obvious however, that for a more detailed transmission coefficient dependence, smaller step between frequencies must be made (note that our step in frequency was 0,25THz), so the resolution is increased.

We believe that small discrepancies (not caused by our approximation i. e. in case of points at frequencies at 5,5; 0,7 and 0,9 THz) of numerical solution from analytical one in figure 21, can be attributed to multiple reflections of the SPP inside of the sample. The existence of these

reflections is supported by the character of the transmission coefficient.

It would seem that other areas of the simulation should be explored further, so that a better precision and higher resolution is obtained. For example, how the simulation size affects the simulation and what effect the boundary conditions have. One could also propose even better SPP generation method which would not generate the spherical wave as well. It is also possible that denser mesh could further improve the results in some cases. Most notably, for frequencies near 1,2THz the mesh density seemed insufficient. However, in chapter 4.1 we have already discussed that this would cause a notable increase in computation time etc. and due to the lack of time we were unable to incorporate these improvements into our simulation.

However, since the simulation generates the SPP, which behaves in accordance to other expected properties (such as shortening of the wavelength of the SPP inside of the sample, phase delay) we believe, that this chapter could be used as an introduction to SPP simulations using Comsol.

4.6. Conclusion

Our main goal in this chapter was to propose a way with which one can excite a surface mode in emw. module of the software Comsol. We have accomplished this using the array of electric dipoles placed inside the metal/dielectric interface which are emitting radiation exhibiting constructive interference along the interface. Consequently, this geometry allows us to impose a wave vector matching the surface plasmon dispersion curve $k = k(\omega)$ for any frequency ω . The generated wave then easily couples to the surface plasmon mode.

Using this method we have excited a SPP and proposed a simulation in which this SPP transmits the sample placed on the metallic substrate. We have seen, that in such a simulation, diffracted waves are generated in points where SPP enters and leaves the sample. This translates into radiative losses, and therefore the amplitude of the electric field of the transmitted SPP is lower than the amplitude of the incident SPP. We have also observed the shift in SPP wavelength inside the sample, which is in accordance with analytical predictions made in figure 18.

The simulation in itself generates results, which are qualitatively predicted by our analytical research. However, since there are discrepancies from our predictions in figure 21 and since the resolution in figure 22 is obviously low, further improvements to the simulation could be made.

We believe that in order to correct this, other areas of the simulation should be explored, i. e. proper boundary conditions and simulation space size could cause the unwanted interference of transmitted wave, therefore hindering the information about the amplitude and phase of this wave. One could also improve the simulation by using a SPP excitation method without exciting the spherical wave. These improvements, together with proper

phase delay calculations, are outside of the scope of this work, since extensive amounts of time would be required to implement all suggestions.

Our simulations could therefore serve as an qualitative description of our experiment, however to obtain quantitative results, improvements to the simulation must be made.

5. The experiment

In this chapter we describe a series of experiments, in which we generated a surface plasmon in the THz spectral range and we detected its propagation along a metal line with or without a bulk dielectric or semiconductor sample wafer positioned onto the metal layer. To this aim we used a set-up for THz transmission spectroscopy at FZÚ ASCR shown in figure 23. In the original set-up a sample wafer for transmittance measurements is inserted to the focal point between the two ellipsoidal mirrors. Within this diploma work we designed an insert which is introduced into the THz beam path near this focal plane. This element directs the THz beam towards a metallic plate and allows us to generate and detect a THz surface plasmon. The side view of this insert is shown in figure 24.

Our experimental set-up is described in scheme below.

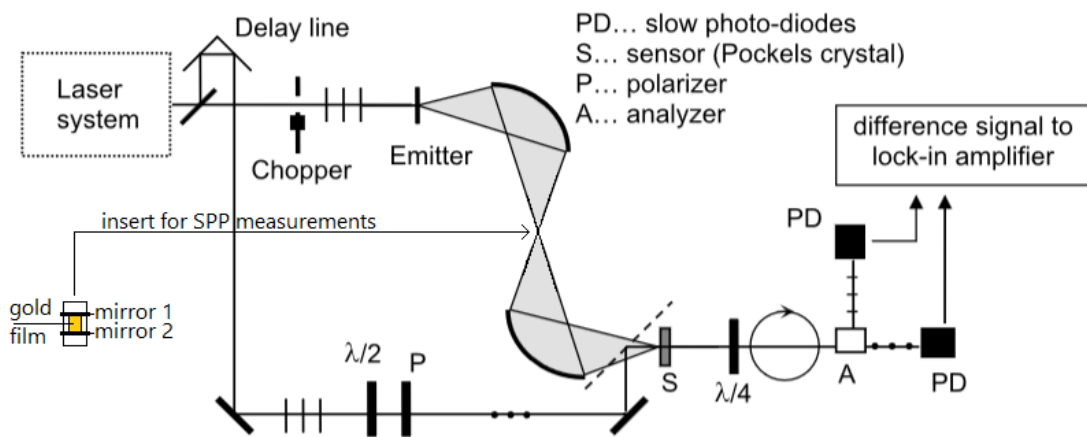


Figure 23: Experimental set-up used to generate the surface plasmon and its measurement – top view. The laser generates fs pulses which are then split in the beam splitter. One branch goes to the THz emitter (in our case the photo-switch [29]) and generates the THz pulse which is then used to excite the SPP. The other pulse is delayed in the delay line. Both pulses then come to the detector, where the delayed optical pulse is used sweep the THz pulse.

Figure 23 describes the top view of our experimental set-up. THz pulse is generated in one of the branches, propagated to the focal area and

then propelled below (using the insert from figure 24), perpendicularly to the sample plane (a plane defined by our metallic layer on which a sample lied) denoted as a rectangle. Here, it is used for the SPP excitation. Close-up of the insert can be seen in figure below.

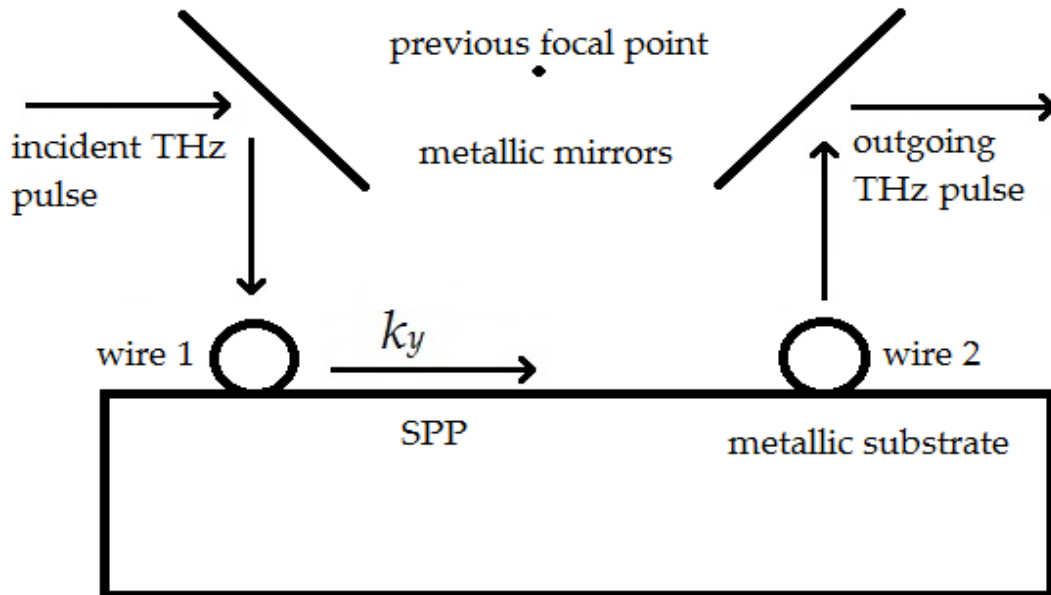


Figure 24: SPP excitation using metallic wires. The distance between wires was 15mm, while their diameter was around $500\mu\text{m}$. Rectangular gold film, deposited on glass served as a metallic substrate. Incident THz pulse is focused onto the wire 1, which then acts like an antenna and starts emitting the radiation, out of which some gets converted into the SPP, propagating in direction perpendicular to wire 1 along the metallic surface. Similar process occurs in wire 2 when the SPP reaches it. Some of the radiation is then incident on the second mirror and propagates to the detector.

We excited the SPP pulse as described in figure 24, which is a side view of the insert from figure 23. As seen in the figure, incident THz pulse is focused onto the metal wire 1 via first metallic mirror. This wire then acts like an antenna and starts emitting THz radiation in all directions, consequently, some of the radiation converts into the SPP propagating along the metallic substrate. The SPP then propagates as a pulse along the surface to the second wire. This wire acts as an antenna too, generating some radiation perpendicular to the metallic surface. The divergent radiated beam is

directed via mirror 2 (fig. 24) towards the second ellipsoidal mirror of the set-up shown in figure 23 and follows the original beam path of the transmission spectrometer up to the sensor. In this sensor an electric field of the pulse in time is measured.

Note, that wires have to be parallel to each other in order to achieve the best results. Using rectangular substrate gave us better control over the parallelism of the wires, since we could simply place them perpendicular to the slip edge, as shown in figure 25.

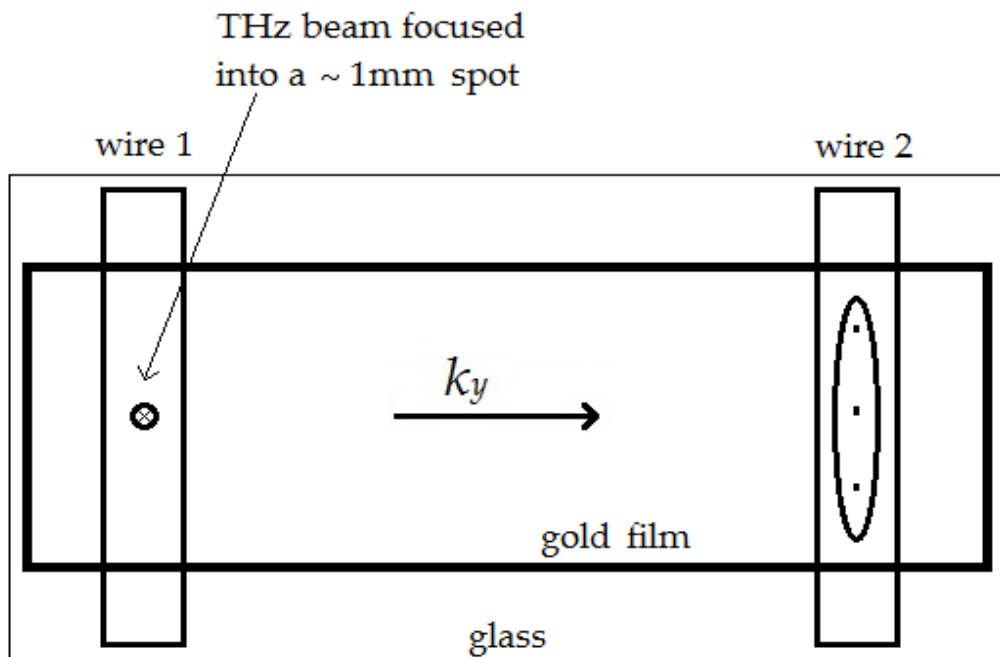


Figure 25: Top view on the wires and metallic substrate from figure 24. SPP propagates perpendicularly to the wire (as shown here by k_y vector). The wires need to be parallel. This is easier to achieve by using rectangular substrate and placing the wires perpendicular to its edge. Note the ellipse on the wire 2 denoting the radiation exiting the SPP mode and propagating perpendicularly to the surface of the substrate into the second mirror from figure 24.

The thickness of the gold substrate was about 200nm which is sufficient since according to [30] the plasma frequency of gold is orders of magnitude higher than the SPP frequency we excited (see figure 27). This means that the penetration depth into the gold is extremely small since we are in the deeply in the Zenneck regime.

5.1. Metal/isotropic dielectric interface results

The first case we will talk about is the metal/isotropic dielectric interface. The dielectric is in our case air. Entire experiment was set up in accordance to figures 24 and 25. Measured electric field of the THz SPP pulse in time can be seen in figure 26. This measurement also served as a reference to all other measurements.

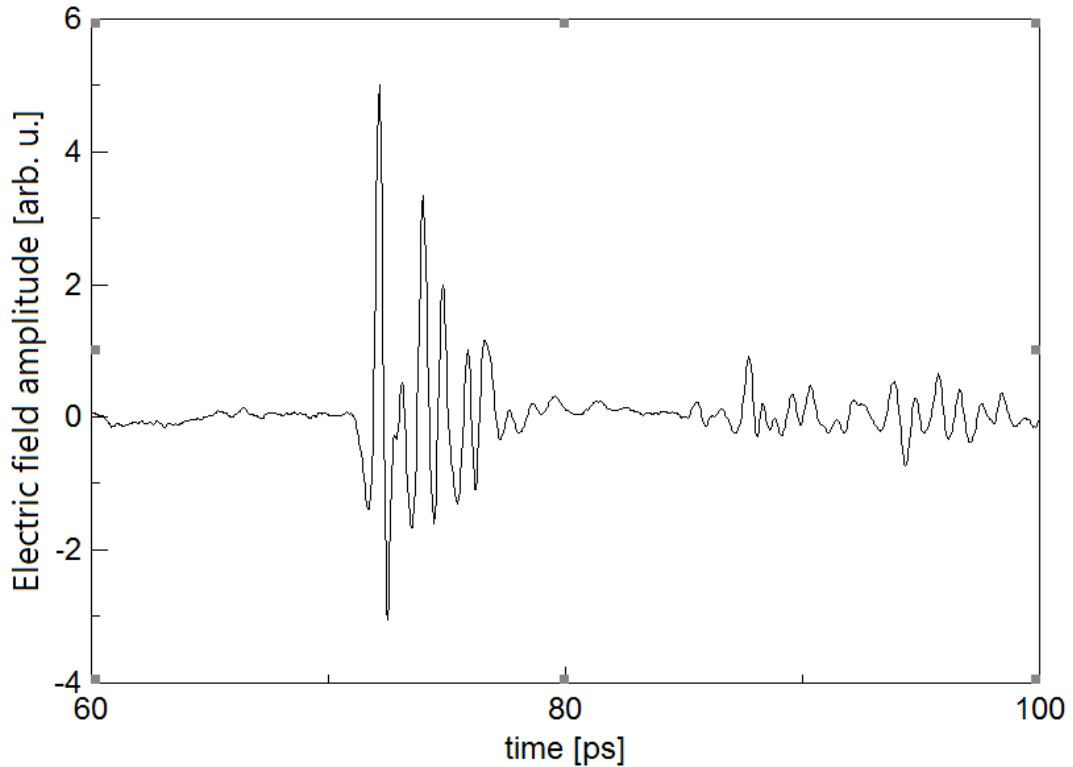


Figure 26: Result of SPP propagating along metal/isotropic dielectric interface measurement. One can see the pulse beginning in the 72nd ps. On the right hand side we can see an artefact.

Since SPP in figure 26 is not necessarily only generated in k_y direction but in $-k_y$ as well (figures 24/25), we believe the mentioned artefact is an SPP reflected off the left edge of the metallic film.

For spectroscopic purposes one needs to know the frequency spectrum of such a pulse, therefore there is a Fourier transformation of this pulse in figure 27. The spectrum shows a sharp maximum close to 1 THz and several side maxima. We think that the character of the spectrum is due to

the resonant character of in- and out- coupling of the surface plasmon.

We believe that this behaviour is caused by our method of excitation of the SPP. Since we are using wires as antennas, it is obvious, that some frequencies are conveyed better than the others. This is supported by a fact, that in [16] it shown that broad-band THz SPP pulse can be generated, without dips in the frequency spectrum by using different excitation method.

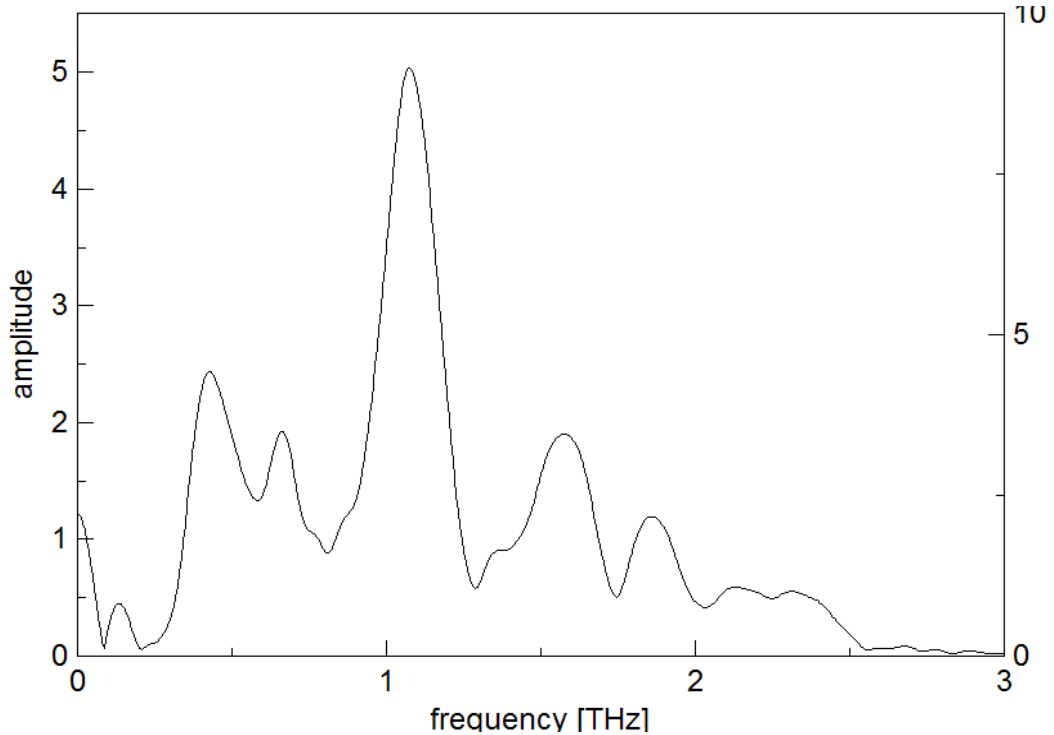


Figure 27: Frequency spectrum of THz SPP pulse shown in figure 26. The Fourier transformation was done only for the pulse in the time window between 80ps and 90ps. Note the dips in the amplitude for certain frequencies, possibly caused by our method of SPP excitation.

Let us note that wires of different diameters were tried as well (diameters of 800 μm and 400 μm) but no significant improvement was observed.

Despite the fact that the shape of the pulse and therefore its frequency spectrum are not ideal, we proceeded to do some basic experiments on the samples of *Si*, *ZnTe*, *GaAs* and a dielectric *Li₂Ge₇O₁₅* (*LGO*). The results are described in the next chapter.

5.2 Measurements on *Si*, *ZnTe*, *GaAs* and *LGO* samples

In these measurements we focused on the phase shift of the propagating surface plasmon upon an insertion of the sample wafer. For each measurement the sample was positioned directly on the metal film and the transmitted surface plasmon was measured. As reference we used the measurement without any sample. The shift in time Δt of the surface plasmon arrival to the sensor with and without sample was determined for each measurement.

To obtain the value of refraction index n we used

$$n = \frac{\Delta t c}{d} + 1 \quad , \quad (54)$$

where d is the sample width of the sample in the k_y direction and c is the speed of light.

Measured data can be seen below.

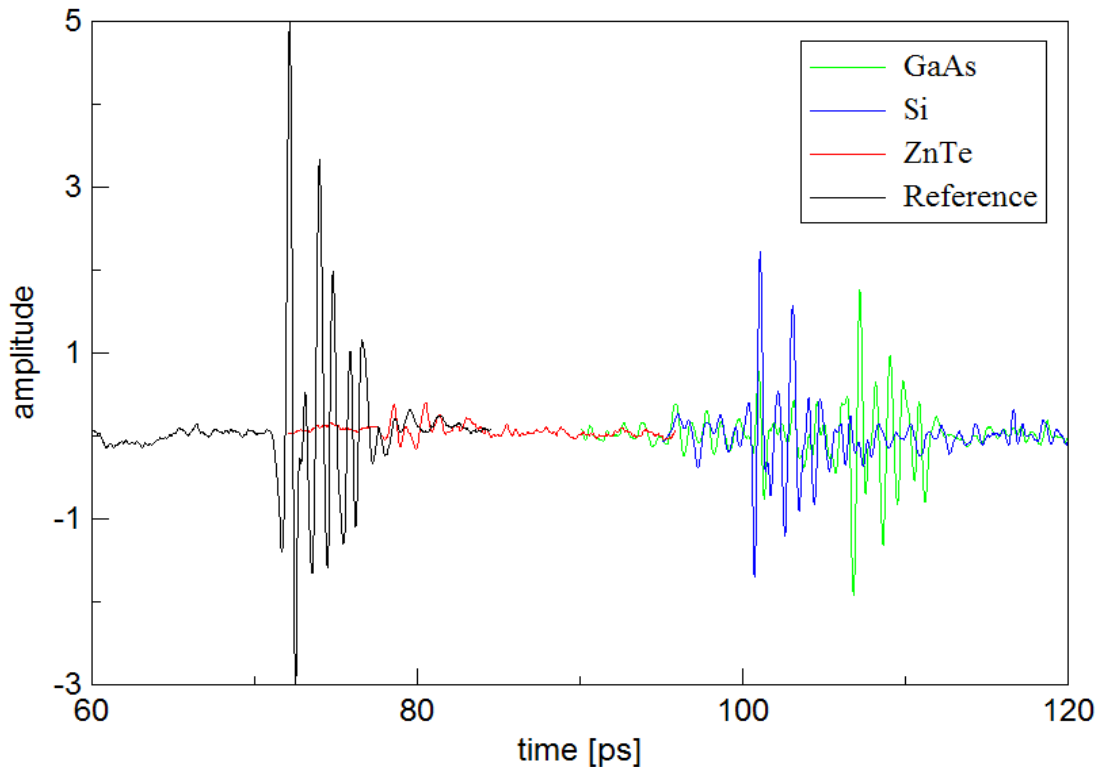


Figure 28: Time shift of the surface plasmon propagation to the sensor due to its propagation in the samples shown in the legend.

The time delay of the wave required for equation (54) was calculated from figure 28. The dimension d of the samples was measured using micrometer screw.

The end results are shown in the table below:

-	Si	ZnTe	GaAs
d [mm]	3,55	0,91	3,95
Δt [ps]	28,6	6,46	34,67
n	3,42	3,13	3,63
Reference n	3,416 [31]	3,13 [32]	3,63 [32]

Table 2 : measured refraction indices for *Si*, *ZnTe* and *GaAs*.

As seen in table 2, our measured refraction indices are in agreement with reference values. Therefore we can conclude that our assumption that we are exciting a surface wave was correct. Note that we used bulk samples with approximate thickness of 1mm. Also note that error of Δt was 0,25ps at worst.

Let us now have a look on the transmission spectra of these samples, obtained as a ratio of the pulse transmitted through the sample and the reference pulse. Both spectra were obtained as a Fourier transformation of the time-domain wave form (strictly speaking, of the part which contains the principal transmitted pulse).

The spectra can be seen in figure 29. There is a lot of noise present and we believe that it is due to the method of SPP excitation we used. This is a possible cause of a nonsensical value of transmission coefficient larger than one in case of *Si*, at around 2THz. Otherwise the spectra should have no prominent features.

We proceeded to measure the anisotropic sample of *LGO*. *LGO* is a weak ferroelectric anisotropic material crystallizing in an orthorhombic structure at room temperature [33]. In particular it features a weak phonon

mode along the polar c-axis [34] at 1.5 THz. This phonon mode is weak and does not cause the permittivity ϵ_c of *LGO* to become negative between ω_0 and ω_L (equation (2)) [18]. However, it should be observed through the attenuation of the surface plasmon mode. On the other hand, no phonon mode should be observed in the THz spectra for polarizations perpendicular to the c axis. In our experiments we first measured a THz spectrum of a plasmon propagating through an *LGO* slab positioned with c-axis perpendicular to the metal surface. In the Zenneck mode of propagation the surface plasmon should be sensitive to the presence of the phonon mode in the material. In the second experiment we positioned the sample slab such that the c-axis was parallel to the metal surface: in the Zenneck regime the phonon mode should not be observed.

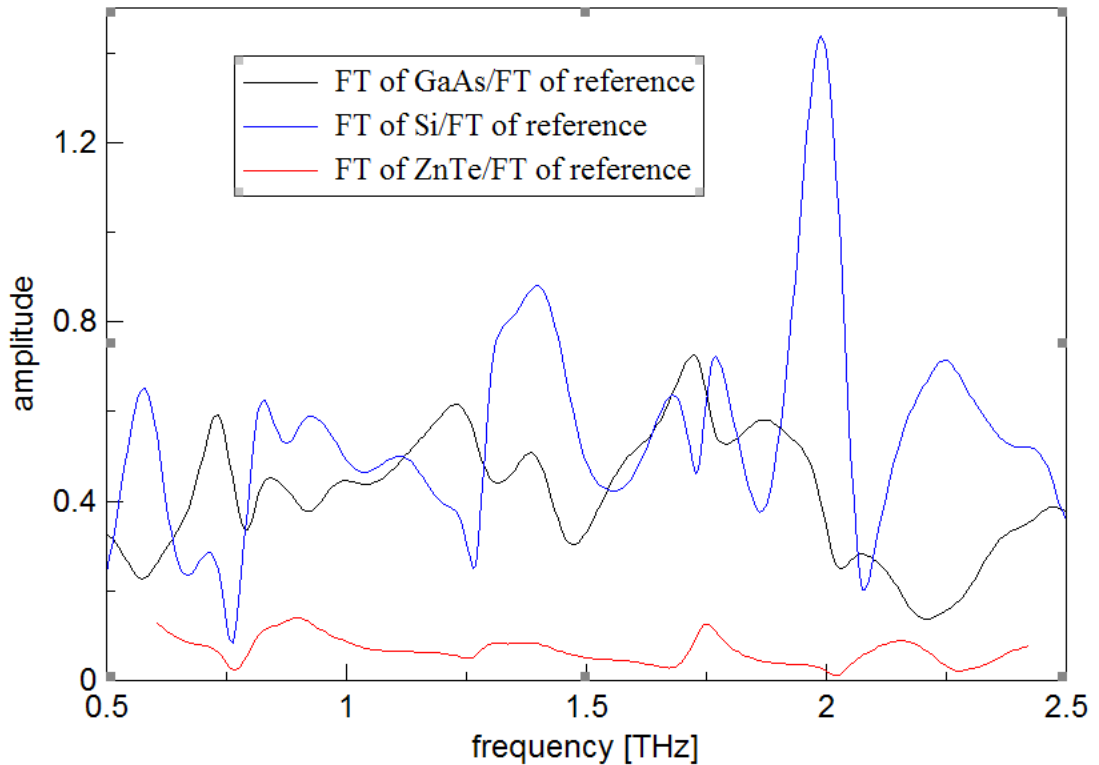


Figure 29: Transmission spectra of samples, denoted in the legend. Since *ZnTe* absorbs THz radiation, the transmission is very low. There are no prominent features in the spectrum of *GaAs*. The peak at 2THz in *Si* curve is caused by the high amount of noise present in all measurements.

The transmission spectra for these two specific orientations of LGO can be seen in figure 30.

Indeed we are able to observe the phonon like resonance. This is an important feat, since it means, that the SPP's are indeed sensitive only to the out-of-plane permittivity of the sample and it would seem that they are suitable for the purposes of THz spectroscopy, at least of bulk samples.

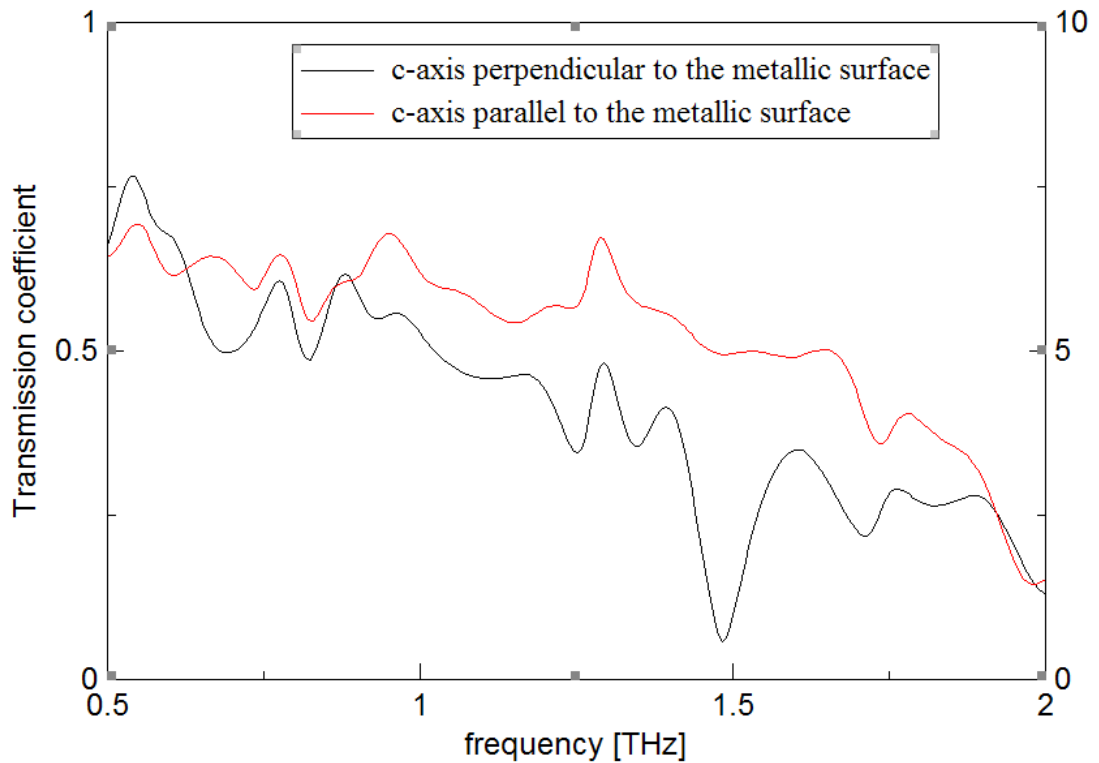


Figure 30: Transmission spectra of LGO for two distinct orientations. In the spectrum of the first orientation – c-axis is perpendicular to the metal's surface - we see an expected phonon like resonance, exhibiting itself as a band gap, at around 1,5 THz. Rotating the sample into a second orientation causes the band gap to disappear.

5.3. Conclusion

In this chapter we have described an experiment in which we excited a SPP wave and used it to perform some basic spectroscopic measurements.

Based on the results in table 2 we indeed believe that we are measuring SPP waves in figures 26 and 28. We have used the data from these figures to evaluate the transmission coefficient of the *Si*, *ZnTe* and *GaAs* samples, shown in figure 29. We also proceeded to the measurement of the anisotropic sample of *LGO* which seems to be promising.

As can be seen in figure 30 we are able to measure different transmission spectra of the *LGO* sample based on its orientation with respect to the SPP polarisation vector.

We believe, that if one were to optimize the in- and out- coupling of the SPP, for example like it is shown in [16], it would be possible to indeed generate a broadband SPP pulse which could then be used for THz SPP spectroscopy as we have shown in this chapter. Moreover, if one would develop more advanced simulations and used them together with said experiment, we are of the opinion, that it should be possible the indeed develop a usable spectroscopic method based on the surface plasmon polaritons.

Thesis conclusion

In this thesis we have analytically described the propagation of surface plasmon polariton along metal/dielectric interfaces using the transfer matrix formalism. Notably, we performed this for both isotropic and anisotropic dielectrics. For uni-axial anisotropic dielectric we proposed an extension of 2x2 transfer matrix formalism for out-of-plane optical axis. The results of our description consist of SPP's dispersion curves. We have also defined two distinct regimes of propagation based on the character of the dispersion curve – the Zenneck regime, where the dispersion is linear, proportional to the out-of-plane refraction index of the superstrate, and the saturated regime, where the dispersion is flat and determined by the product of in-plane and out-of-plane dielectric components.

We concluded that in case of anisotropic dielectric, the SPP propagating in the Zenneck regime is only affected by the out-of-plane permittivity of the dielectric. In case of the SPP propagating along metal/dielectric layer interface we have found out that for thin layers the Zenneck regime is dominated by the superstrate's permittivity. The permittivity of the layer is only accessible for thick layers in Zenneck regime. Since the Zenneck regime is dependent on the out-of-plane permittivity, and because of perpendicular polarization of SPP (with respect to interface) in Zenneck regime we concluded, that the Zenneck regime is suitable for spectroscopic purposes in THz spectral range.

We used these conclusions in our experimental measurements. We proposed a scheme for surface plasmon excitation using wires as an antennae. The propagation of SPP along metal/dielectric interface was studied. Most notably, the sample of anisotropic dielectric $Li_2Ge_7O_{15}$ was measured. We observed a soft phonon mode along the polar c-axis of this

material, translating into a absorption line in the transmission spectrum. On the other hand, no absorption line was observed in the THz spectrum for polarizations perpendicular to the c axis, where no phonon modes exist in the THz range.

Moreover we carried out a numerical simulation of said experiment, but we were only able to obtain qualitative results. To obtain quantitative results, improvements to the simulation must be made.

In conclusion, we believe we have shown, that the surface plasmon polaritons have the potential to be used in spectroscopic measurements in the THz spectral range, while their most notable application covers the measurement of the out of plane response of dielectric materials, as shown in our measurement of the $Li_2Ge_7O_{15}$ sample.

References

- [1] R. W. Wood. On a remarkable case of uneven distribution of light in a diffraction grating spectrum. *Phil. Mag.* 1902, **4**, 396.
- [2] Lord Rayleigh. Dynamical theory of the grating. *Proc. Roy. Soc.* 1907, **A79**, 399.
- [3] C. J. Powell, J. B. Swan. Effect of oxidation on the characteristic loss spectra of aluminum and magnesium. *Phys. Rev.* 1960, **118**, 640.
- [4] E. Kretschmann, H. Reather. Radiative decay of nonradiative surface plasmon excited by light. *Z. naturforssch.* 1968, **23a**, 398.
- [5] A. Otto. Excitation of nonradiative surface plasma waves in silver by the method of frustrated total reflection. *Z. Phys.* 1968, **216**, 398.
- [6] J. Homola, S. S. Yee, G. Gauglitz. Surface plasmon resonance sensors: review. *Sensors and Actuators B: Chemical.* 1999, **54**, 3.
- [7] B. Špačková. Optical sensors based on surface plasmons. Prague, 2014. Abstract of dissertation. Faculty of Nuclear Sciences and Physical Engineering, Czech Technical University in Prague.
- [8] Pierre Berini. Long-range surface plasmon polaritons. *Advances in Optics and Photonics 1.* 2009, **1**, 484-588.
- [9] Jesly Jacob et al. Propagation of surface plasmon polaritons in anisotropic MIM and IMI structures. *Superlattices and microstructures.* 2008, **44**, 282-290.
- [10] A. Sommerfeld. *Ueber die fortpflanzung elektrodynamischer wellen längs eines drahtes.* *Ann. Phys. Chem.* 1899, **67**, 233.
- [11] J. Zenneck. *Ann. Phys.* 1907, **23**, 846.
- [12] K. Wang, D. M. Mittleman. Metal wires for terahertz wave guiding. *Nature.* 2004, **432**, 376.
- [13] T.-I. Jeon, J. Zhang, and D. Grischkowsky. THz sommerfeld wave

propagation on a single metal wire. *Appl. Phys. Lett.* 2005, **86**(16), 161904.

[14] T.-I. Jeon, D. Grischkowsky. THz Zenneck surface wave (THz surface plasmon) propagation on a metal sheet. *Appl. Phys. Lett.* 2006, **88**, 061113.

[15] John F. O'Hara et al. Terahertz surface plasmon polariton coupling on metallic grating. *OPTICS EXPRESS*. 2004, vol. 12, issue 25, 6397-6402.

[16] John F. O'Hara et al. Prism coupling to terahertz surface plasmon polaritons. *OPTICS EXPRESS*. 2005, vol. 13, issue 16, 6117-6126.

[17] J.B. Pendry, A.J. Holden, D.J. Robbins, W.J. Stewart. *J. Phys: Condens. Matter*. 1998, **10**, 4785.

[18] J. B. Pendry et al. Mimicking Surface Plasmons with Structured Surfaces. *Science*. 2004. 1098999.

[19] Kai-Erik Peiponen, J. Axel Zeitler, Makoto Kuwata-Gonokami. *Terahertz Spectroscopy and Imaging*. Springer – Verlag Berlin Heidelberg 2013. ISBN: 978-3-642-29564-5

[20] Stefan A. Maier et al. Terahertz Surface Plasmon-Polariton and Focusing on Periodically Corrugated Metal Wires. *Physical review letters*. 2006, PRL 97. 176805.

[21] T. W. Ebbesen, H. J. Lezec, H. F. Ghaemi, T. Thio, P. A. Wolff. Surface plasmons enhance optical transmission through subwavelength holes. *Phys. Rev. B*. 1998, **58**, 6779-6782.

[22] C. Kadlec, V. Skoromets, F. Kadlec, H. Němec, J. Hlinka, J. Schubert, G. Panaitov, P. Kužel. Temperature and electric field tuning of the ferroelectric soft mode in a strained SrTiO₃ / DyScO₃ heterostructure. *Phys. Rev. B*. 2009, **80**, 174116.

[23] V. Skoromets, C. Kadlec, J. Drahoukoupil, J. Schubert, J. Hlinka, P.

Kužel. Systematic study of terahertz response of SrTiO₃ based heterostructures: Influence of strain, temperature, and electric field. *Phys. Rev. B*. 2014, **89**, 214116.

[24] J. H. Haeni, W. Chang, R. Uecker, P. Reiche, Y. L. Li, S. Choudhury, W. Tian, M. E. Hawley, B. Craigo, A. K. Tagantsev, X. Q. Pan, S. K. Streiffer, L. Q. Chen, S. W. Kirchoefer, J. Levy, D. G. Schlom. *Nature*. 2004, **430**, 758.

[25] I. Lukyanchuk, A. Pakhomov, A. Sené, S. Sidorkin, V. Vinokur. Terahertz electrodynamics of 180 domain walls in thin ferroelectric films. arXiv: 1410.3124v3

[26] N. W. Ashcroft, N. D. Mermin. *Solid State Physics*. United States of America: Thomson Learning, Inc. 1976. 826 s. ISBN 0-03-083993-9

[27] F. Pedrotti, L. Pedrotti. Introduction to optics, second edition. Prentice-Hall, Inc. 1993. ISBN 0-13-016973-0

[28] COMSOL Inc. COMSOL Multiphysics. [online]. In 2016 by COMSOL Inc. Dostupné z <https://www.comsol.com/comsol-multiphysics> [cit 5.5.2016]

[29] A. Dreyhaupt, S. Winnerl, T. Dekorsy and M. Helm. High-intensity terahertz radiation from a microstructured large-area photoconductor. *Appl. Phys. Lett.* 2005, **86**, 121114.

[30] K. Murata, H. Tanaka. Surface-wetting effects on the liquid-liquid transition of a single-component molecular liquid. *Nature Communications*. 2010, **1**, article number: 16.

[31] R. H. Giles. *Characterisation of Material Properties at Terahertz Frequencies*. Submillimeter Technology Laboratory, University of Massachusetts, Lowell. 1995.

[32] O. Ostroverhova. *Handbook of organic materials for optical and*

(opto)electronic devices, Properties and applications. Woodhead Publishing Limited. 2013. ISBN 978-0-85709-876-4.

[33] F. Kadlec, J. Petzelt, V. Železný, and A. A. Volkov. *Solid State Commun.* 1995, **94**, 725.

[34] P. Kužel and J. Petzelt. *Ferroelectrics.* 2000, **239**, 949-956.